EVOLUTION OF ASYMPTOTIC GIANT BRANCH STARS

Falk Herwig

Los Alamos National Laboratory, Los Alamos, New Mexico 87545; email: fherwig@lanl.gov

Key Words stellar evolution, low- and intermediate-mass stars, nucleosynthesis, *s* process

■ **Abstract** The current status of modeling the evolution and nucleosynthesis of asymptotic giant branch (AGB) stars is reviewed. The principles of AGB evolution have been investigated in recent years leading to improved and refined models, for example with regard to hot-bottom burning or the third dredge-up. The postprocessing *s*-process model yields quantitative results that reproduce many observations. However, these and most other processes in AGB stars are intimately related to the physics of stellar mixing. Mixing in AGB stars is currently not well-enough understood for accurate yield predictions. Several constraints and methods are available to improve the models. Some regimes of AGB evolution have not yet been studied in sufficient detail. These include the super-AGB stars and AGB stars at extremely low or ultra low metallicity.

1. INTRODUCTION

Asymptotic giant branch (AGB) stars are the final evolution stage of low- and intermediate-mass stars driven by nuclear burning. This phase of evolution is characterized by nuclear burning of hydrogen and helium in thin shells on top of the electron-degenerate core of carbon and oxygen, or for the most massive super-AGB stars a core of oxygen, neon, and magnesium. In particular, the recurrent thermonuclear flashes that induce a complex series of convective mixing events provide a rich environment for nuclear production. The nucleosynthesis in AGB stars plays an important role for our understanding of the origin of the elements. AGB stars are the major contributors to the integral luminosity of intermediate-age stellar systems. For that reason they are an important tool to study extra-galactic populations (Battinelli & Demers 2004).

Prior to the AGB phase low- and intermediate-mass stars follow a characteristic evolutionary track in the $\log T_{eff} - \log L$ diagram (Hertzsprung-Russell diagram, HRD). Such a complete evolution track is shown in Figure 1 for an initial stellar mass of $2\,M_{\odot}$. The evolution starts after the star formation and pre-main-sequence evolution with the core H-burning phase (observationally the main sequence). When all H is transformed into He in the core, nuclear energy release ceases and
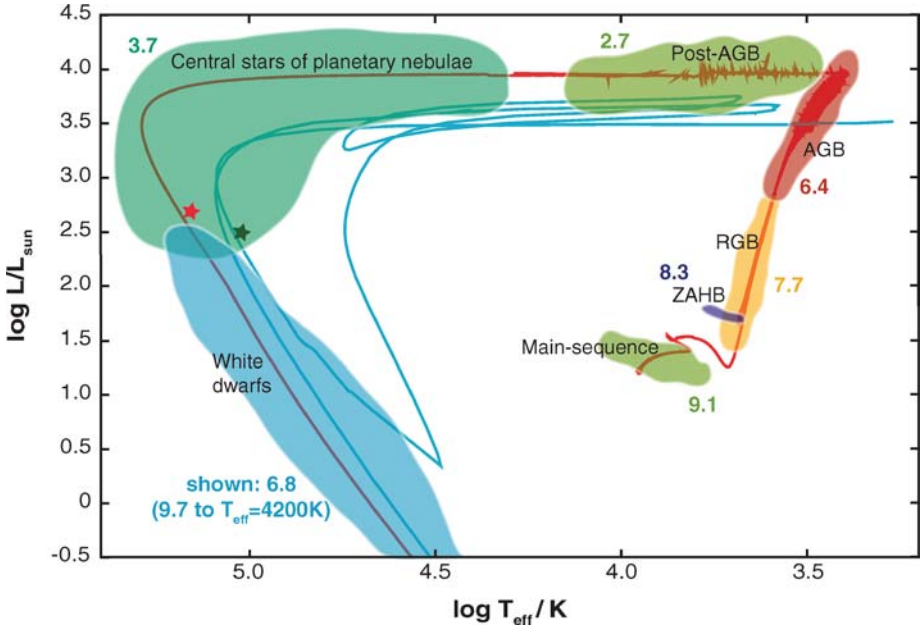
Figure 1   Hertzsprung-Russell diagram of a complete 2 $M_\odot$ evolution track for solar metallicity from the main sequence to the white dwarf evolution phase. In the cooler section of the post-AGB phase, wiggles in the track are caused by numerical convergence difficulties. The *blue* track shows a born-again evolution (triggered by a very late thermal pulse, Section 4.2) of the same mass, however, shifted by approximately $\Delta \log T_{\mathrm{eff}} = -0.2$ and $\Delta \log L/L_\odot = -0.5$ for clarity. The *red* and *green* stars mark the position of the central stars of planetary nebulae for which spectra are shown in Figure 8 (see Section 4.2). The number labels for each evolutionary phase indicates the log of the approximate duration for a 2 $M_\odot$ case. Larger or smaller mass cases would have smaller or larger evolutionary timescales, respectively.

the core starts to resume gravitational contraction. H burning now starts in a shell around the He core, and in the HRD the star evolves quickly to the base of the Red Giant Branch (RGB). As the core continues to contract, the envelope of the giant expands and the H-shell luminosity grows. The star climbs up the RGB, or first giant branch. The star is cool and the entire envelope is convectively unstable. The associated mixing leads to observable abundance variations along the RGB. The ignition of core He burning depends on the intial mass (Figure 2). If the initial mass is less than approximately 1.8 $M_\odot$ the He core has become electron-degenerate when the star evolves to the tip of the RGB. These stars experience a degenerate core He flash and settle afterwards in quiescent He-core burning on the zero-age horizontal branch (ZAHB). Initially, more-massive stars ignite He burning in the core in a nonviolent mode and like less-massive stars continue their evolution in the horizontal branch.
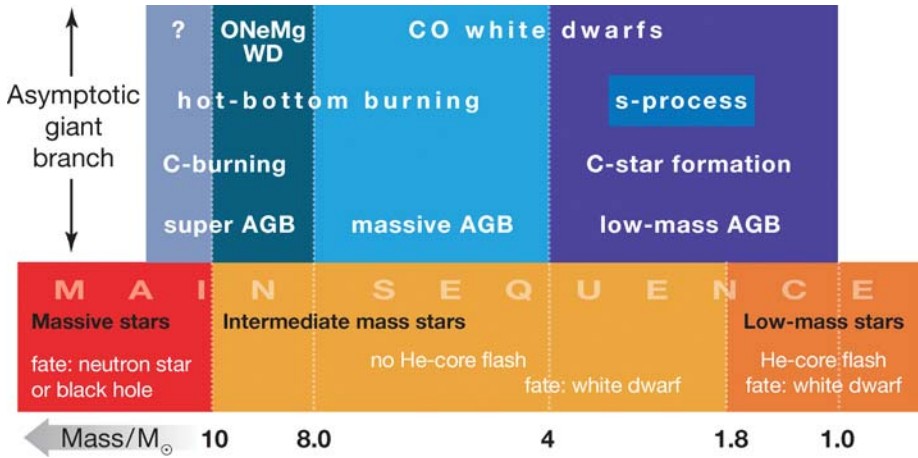
Figure 2 Classification of stars by mass on the main sequence (*lower part*) and on the AGB (*upper part*). The *lower part* shows mass designation according to initial mass. The *upper part* indicates the mass classification appropriate for AGB stars. Approximate limiting masses between different regimes are given at the bottom. These estimates are dependent on physics assumptions and input of models, as well as on metallicity. The different regimes have been labeled with some characterizing properties. The evolutionary fate of super-AGB stars is still uncertain (Section 5).

The He-core burning phase is about a factor of 10 shorter than the H-core burning phase. He-core burning leaves a C/O core behind that is surrounded by both a He- and a H-burning shell. For stars with initially less than 8 $M_\odot$ carbon does not ignite, and the C/O core contracts and becomes increasingly electron-degenerate. During the early AGB phase, the He shell dominates nuclear production. It burns outward in mass and reaches the H shell. At that point, nuclear energy release is dominated by the H shell and interrupted periodically by thermonuclear runaway He-shell flash events that initiate a complex series of convective and other mixing events (Figure 3).

The evolution sequences shown in Figure 1 are computed by solving numerically the fundamental equations of stellar structure and evolution (hydrostatic equilibrium, mass conservation, energy generation, and transport). A stellar evolution sequence consists of several ten thousand adaptive time steps. Details on the input physics and modeling assumptions with particular relevence to the modeling of AGB stars are given in Section 2.1. A review of the evolution and explosion of massive stars can be found in Woosley, Heger & Weaver (2002).

A review of the evolution of AGB stars was presented in this series by Iben & Renzini (1983) more than 20 years ago. Several aspects or related issues have been covered since by review articles in this series, like mass loss (Willson 2000), the *s* process (Busso, Gallino & Wasserburg 1999; Meyer 1994), and the
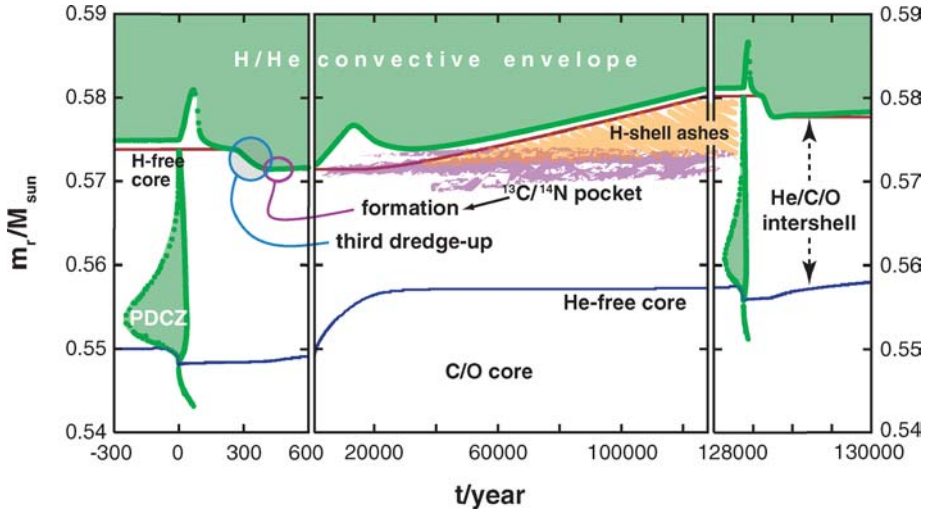
Figure 3 Thermal pulse 14, the subsequent interpulse phase and thermal pulse 15 of 2 $M_\odot$, $Z = 0.01$ sequence ET2 of Herwig & Austin (2004). The timescale is different in each panel. The *red solid line* indicates the mass coordinate of the H-free core. The *dotted green line* shows the boundaries of convection; each *dot* corresponds to one model in time. Convection zones are *light green*. The shown section of the evolution comprises 12,000 time steps. The colors indicating convection zones, layers with H-shell ashes and the region of the ^{13}C pocket match those in Figure 5.

post-AGB stars and their observational implications for the *s*-process (van Winckel 2003). In recent years several summaries of the properties of new models have appeared in conference proceedings (Lattanzio & Boothroyd 1997, Blöcker 1999, Herwig 2003b). A textbook on AGB stars is now available and covers the basics of the interior evolution and the atmosphere, circumstellar, and other observational properties (Habing & Olofsson 2004). This review describes the new detailed picture of the interior evolution and nucleosynthesis that is now emerging.

According to model calculations, thermal-pulse AGB evolution is strongly mass dependent. For example dredge-up efficiency, the *s* process, C-star formation, or hot-bottom burning are strongly correlated with specific initial mass ranges. Therefore different evolutionary properties of AGB stars can be classified according to mass, and a schematic overview is given in Figure 2. Generally stars are broadly distinguished by their initial masses as massive, intermediate, and low-mass stars. Here low-mass stars may be designated to have $M < 1.8\,M_\odot$ (depending on overshoot mixing), ignite He-core burning under degenerate conditions in a flash, and end their lives as white dwarfs. Intermediate-mass stars ignite He in the nondegenerate core and end their lives as white dwarfs, and massive stars are those massive enough to explode as a supernova. This classification is not useful for thermal-pulse AGB stars. For example, the *s*-process' nuclear production site consists of

low-mass AGB stars, which includes stars up to a mass of initially $\sim$3 $M_\odot$ (Busso, Gallino & Wasserburg 1999). Observers describing a star (or a damped Ly-α system) with a large nitrogen abundance may consider the role of intermediate-mass stars, excluding all stars below initially 4 $M_\odot$ that do not experience efficient hot-bottom burning. For AGB stars the following classification is recommended and adopted in this review. Low-mass AGB stars do not experience hot-bottom burning, whereas massive AGB stars do. Those intermediate-mass stars that can ignite carbon and have a sub-Chandrasekhar H-free core after the second dredge-up are super AGB stars. Some of these may core collapse into a neutron star; some will evolve into the most massive white dwarfs with ONeMg cores. Thus, all massive AGB stars have initially intermediate-mass stars as progenitors, and some low-mass and some intermediate-mass stars become low-mass AGB stars. The stars of very low mass may never reach the AGB. The most massive intermediate-mass stars may become super-AGB stars.

Most of the basic evolutionary features of thermal-pulse AGB stars were established qualitatively in the review by Iben & Renzini (1983). Improvements have been achieved since then in virtually all aspects of standard AGB models. Properties and modeling techniques of AGB stars are described in Section 2 and include the important question of the third dredge-up. One of the most interesting aspects of AGB stars is the fact that they harbor the nuclear production site of the *s* process. Because of its importance the most recent development since the review by Busso, Gallino & Wasserburg (1999) is summarized in Section 3 with a focus on mixing processes. This discussion includes the effect of rotation, which has only recently been considered for AGB stars. Modeling of the *s* process in conjunction with the high-accuracy data from laboratory measurements of presolar meteoritic grains (Zinner 1998) open a new avenue for testing physics assumptions in stellar evolution that are potentially relevant for the evolution of the massive supernova progenitors as well. In the new framework of stellar evolution of AGB stars, full model sequences from the main sequence to the faint white dwarf evolution stage can be followed on a fairly routine basis. This makes observational properties of progenitors and progeny of AGB stars available as valuable constraints for further improvements of models (Section 4). Both the constrains from grains and from AGB progeny and progenitors will eventually be useful when constructing stellar evolution of super-AGB stars (Section 5) and in the extremely metal-poor regime (Section 6). In particular, many qualitatively new observations of stars with very low metallicity are now emerging, and the comparison with initial attempts to model the evolution appears to raise many new questions.

2. PROPERTIES OF AGB STARS AND MODELS

Low- and intermediate-mass stars evolve through H-core burning on the main sequence, followed by the RGB evolution and He-core burning on the horizontal branch (Figure 1). Then follows the evolution up the AGB with the characteristic
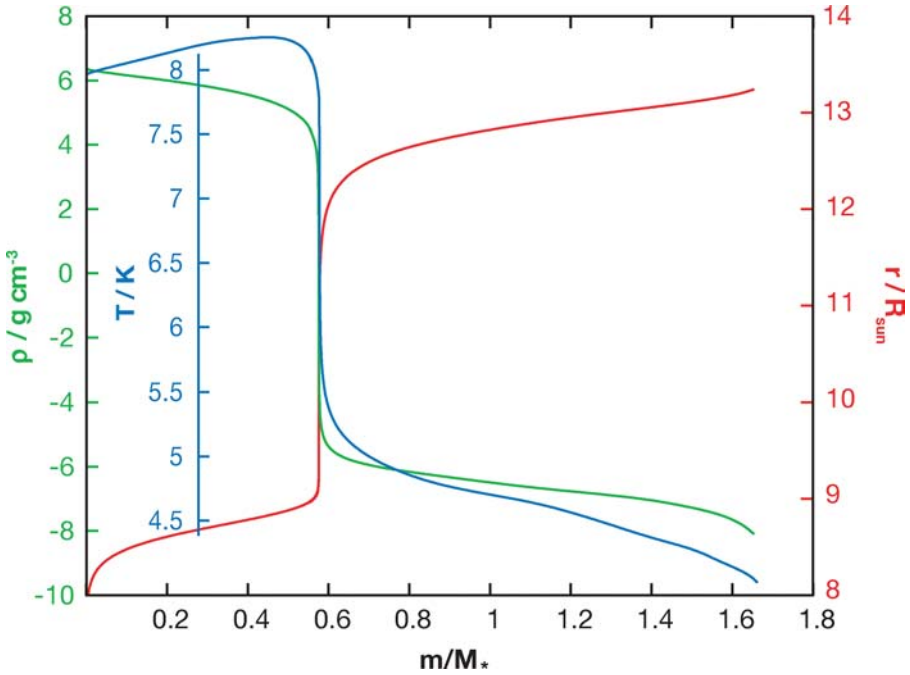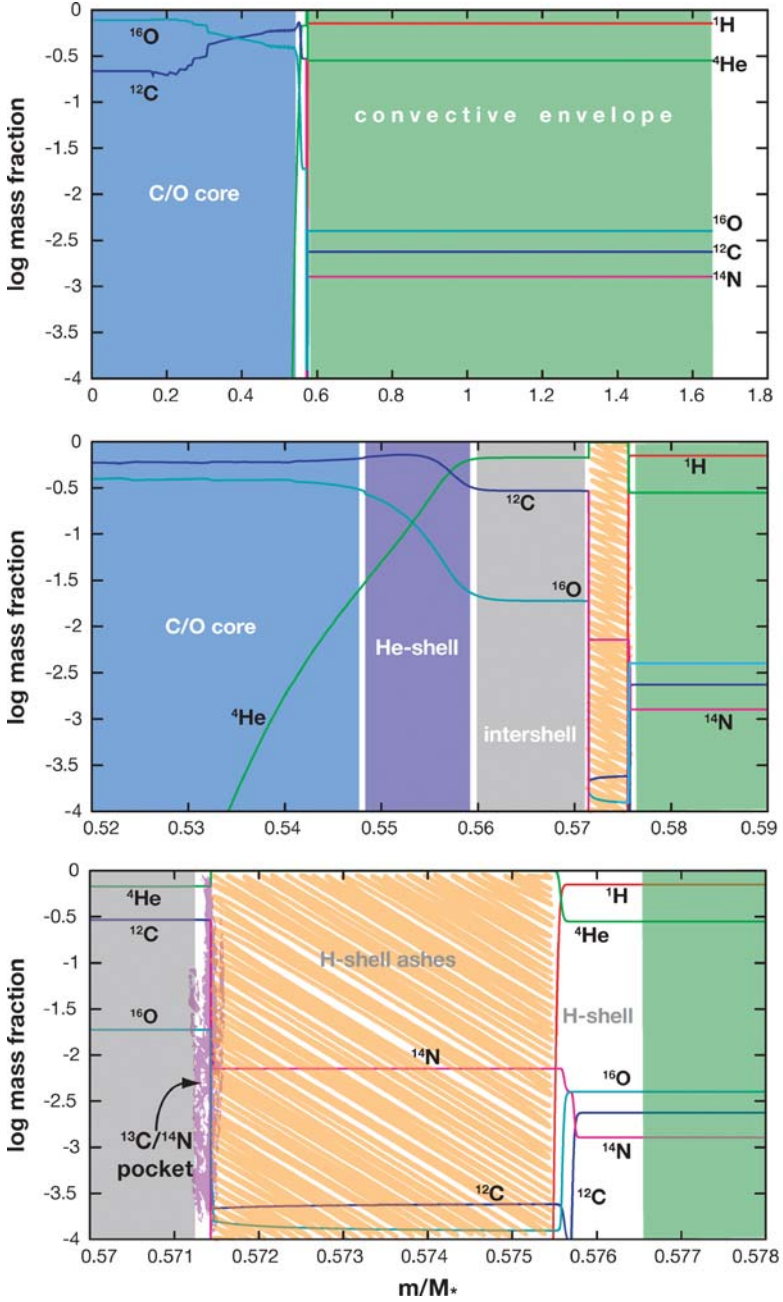
Figure 4   Structural profile of stellar model 46000 of sequence ET2 ($2\,M_\odot$, $Z = 0.01$) of Herwig & Austin (2004), corresponding to $t = 76000$ yr in Figure 3.

thermal pulses during the advanced AGB phase. Increasing mass loss leads to the ejection of the envelope. This promotes the post-AGB evolution and finally the central star of planetary nebulae and white dwarf evolution phases.

AGB stars have a unique structural makeup (Figure 4). The core is basically a preformed C/O white dwarf with a mass of $\sim 0.5 \ldots 1.0\,M_\odot$. More massive white dwarfs are known observationally (Należyty & Madej 2004) in significant numbers. According to stellar-evolution models their internal composition is O, Ne, and Mg, and their progenitors are the super-AGB stars (García-Berro & Iben 1994). Larger samples of white dwarfs will show if single stars with initially $8 \ldots 10\,M_\odot$ are the dominant evolutionary channel for these objects. Apart from Section 5 this review deals exclusively with C/O-core AGB stars.

The tiny core is surrounded by an extended giant envelope filling the stellar radius of several hundred $R_\odot$. Nuclear processing of hydrogen and helium takes places in two spherical shells on top of the core (Figures 3 and 5). The final phase of AGB evolution is characterized by recurrent thermal pulses. These thermonuclear flashes of burning shells on degenerate cores are in fact quite common, and are also known, for example, to occur in the form of X-ray bursts in accreting neutron stars (Woosley et al. 2004). The instability is caused by a combination of the thin-shell instability and partial degeneracy (Kippenhahn & Weigert 1990; Yoon, Langer

Figure 5 Chemical profile (H, He, C, N, O) of stellar model 46000 of sequence ET2 (2 $M_{\odot}$, $Z = 0.01$) of Herwig & Austin (2004), corresponding to $t = 76000$ yr in Figure 3.

& van der Sluys 1994). In AGB stars the He-shell flash arises after a prolonged quiescent interpulse phase during which the dormant He shell accretes helium from the dominant nuclear source, the H shell. The large energy generation of the He shell during the flash is driven mainly by the triple-α reaction and induces a temporary convective instability throughout the region between the shells (the intershell). This pulse-driven convection zone (PDCZ) is important for the nuclear production in AGB stars because the highest temperatures for nucleosynthesis are reached at its base ($\sim 3 \cdot 10^8$ K).

Nucleosynthesis in AGB stars includes H and He burning, but not C burning (except for the super-AGB stars, see Section 5). Hot-bottom burning in more massive AGB stars (Section 2.5) can modify the isotopic—and sometimes for lower-mass species, the elemental—abundances of Ne to Si. However, all other synthesis of heavier elements, in particular the trans-iron elements, is due to the s process (Section 3).

2.1. Input Physics

The evolution of thermal-pulse AGB stars is simulated with 1D, adaptive grid, Lagrangian, hydrostatic or hydrodynamic evolution codes (for synthetic or post-processing models see Section 2.6). The basic stellar evolution equations as well as fundamental processes are covered, for example, in the text book by Kippenhahn & Weigert (1990). Numerical models have typically 2000 grid points. A stellar equation of state provides for ideal gas with radiation pressure and is corrected for (partial) ionization, (partial) electron-degeneracy, and Coulomb interaction (for example, Forestini & Charonnel 1997, Stolzmann & Blöcker 2000). For the evolution of AGB cores, heat conduction and neutrino losses are taken into account (Itoh et al. 1996). Most 1D stellar-evolution codes use the mixing-length theory (MLT) to describe the effect of mixing. Attempts to improve this situation has lead to the full-spectrum convection theory of Canuto & Mazzitelli (1991) with implications for AGB evolution in particular in the case of hot-bottom burning (Section 2.5).

All charged particle reactions are now followed with sufficiently large nuclear networks in AGB evolution calculations. For example Forestini & Charbonnel (1997) use a network with 45 nuclides (including 13 radioactive species) and 172 nuclear and decay reactions. They were the first to present a set of yields for this large number of species from full stellar evolution calculations. The evolution was followed from the main sequence into the thermal-pulse regime including a few pulses. At this point many evolution sequences enter an asymptotic regime, which is characterized by a linear time dependence of many structural properties like the core-mass or the interpulse H-shell peak luminosity. For this regime Forestini & Charbonnel (1997) have obtained the abundance evolution from a synthetic extrapolation (Section 2.6).

In this work the network included a simple neutron sink, and neutron-capture reactions on light species were considered. This is particularly important for

extremely metal-poor AGB models (Section 6) where some n-heavy species like ^{23}Na or ^{26}Mg are significantly effected by n-capture reactions (Herwig 2004c). A two-reaction heavy neutron sink was introduced by Herwig, Langer & Lugaro (2003). It consists of two artificial particles. One particle that we called G represents the total number of nuclei generated by the heaviest species considered explicitly in the network; the other, which we called L, counts the number of neutrons captured by all nuclei represented by the first artificial particle. For example, Herwig, Langer & Lugaro (2003) included ^{62}Ni as the heaviest isotope terminating the explicit accounting of the iron group elements. Then, the first neutron-sink reaction is ^{62}Ni(n, γ)^{63}G and the second is ^{63}G(n, ^{1}L)^{63}G. This prescription conserves baryonic mass and allows some estimate of the *s*-process strength as given by the number n_{cap} of neutrons captured by each iron particle. If one choses the G-particle to represent everything heavier than and including ^{56}Fe, then ^{1}L/^{63}G = n_{cap}.

For most stages of thermal-pulse AGB stars abundance mixing and nuclear burning can be treated separately (operator split). However, during hot-bottom burning in more massive AGB stars as well as during particular evolution events in extremely low-metallicity AGB stars a simultaneous solution of the nuclear network and the time-dependent mixing equations, or some equivalent scheme, is required.

Recent AGB models use the tabulated OPAL96 opacities of Iglesias & Rogers (1996), which are available for a range of metallicities. Although the base mixture is a solar-scaled abundance distribution the standard set of tables accounts for primary carbon and oxygen in variable proportions to replace H and He. This is particularly useful for AGB stars in which the third dredge-up can enrich the envelope with carbon and oxygen and even reverse the C/O ratio from solar to above unity. The OPAL opacities must be complemented with tables for low temperatures containing the regime of molecular contributions. Recent models use the tables by Alexander & Ferguson (1994). However, these do not allow for changes in the C and O abundance at the stellar surface owing to internal nucleosynthesis processes. This appears to be a physics input that must be improved in future AGB calculation. Marigo (2002) showed that the effect of molecular opacities with variable C/O ratio helps account for a number of observational properties of C stars. For C/O < 1, carbon atoms are almost exclusively locked in the CO molecules that have a low condensation temperature. When the C/O ratio exceeds unity as a result of the third dredge-up, carbon can form molecules that are absent during the preceeding O-rich phase. Most notably, CN has been identified by Marigo (2002) to add important opacity to the atmosphere of C stars. This leads to a sudden and marked decrease of the effective temperature by $\Delta T_{eff} \sim 300$ K, depending on mass.

Such a pronounced temperature decrease leads to substantial increase of mass loss when the star becomes a C star. Pulsating wind models in which the mass loss is driven by radiation pressure on dust grains predict that the mass loss depends strongly on the temperature. Wachter et al. (2002) derive a mass-loss formula from their pulsating wind models in which the temperature enters with an exponent of -6.81. This translates for low-mass AGB stars to a mass-loss increase of a factor

of $2.5 \cdots 3.0$ when they become C rich. The lower temperatures and increased mass loss for C-star AGB stars has many implications. This effects the number ratio of C to S and M stars in old- and intermediate-age stellar populations, the nucleosynthetic yields, the interpretation of color-color diagrams of O-rich and C-rich stars, the *s*-process nucleosynthesis (Section 3), as well as the maximum C/O ratio that can be obtained (Section 2.4). For example, if the the mass loss for C stars is larger, then fewer thermal pulses can occur during the C-star phase. Correspondingly less nucleosynthesis can take place during the C-rich phase. In the synthetic models (Section 2.6) of Marigo (2002) with mass loss (Vassiliadis & Wood 1993) and C/O ratio–dependent molecular opacity, an AGB star with intially 2 $M_\odot$ makes 18 thermal pulses as an O-rich star, followed by 6 thermal pulses as a C star. In comparison, the 2 $M_\odot$ stellar evolution AGB calculation for $Z = 0.01$ of Herwig & Austin (2004, sequence ET2) with mass loss (Blöcker 1995, scaled with a factor 0.1) but without the C/O ratio–dependent molecular opacities, evolves through 12 thermal pulses before it becomes a C star and all mass is lost after 6 additional pulses.

2.2. Dredge-Up

Dredge-up is the convective mixing process that brings material processed by nucleosynthesis to the surface, where it can be observed and ejected into space through wind mass loss. Post-main-sequence stellar configurations have a core inside the nuclear burning shell and an envelope outside the shell. Dredge-up occurs when the envelope expands and cools as the core contracts after the end of a dominant nuclear burning event. For example, the first dredge-up refers to the deepening convective envelope after the end of H-core burning. The second dredge-up refers to the descending convective instability after the end of He-core burning. Each thermal pulse on the AGB provides similar favorable conditions for the convective dredge-up of material after the end of the flash-burning in the He shell. This third dredge-up brings primary nucleosynthesis products from combined H-shell and He-shell burning to the surface. These products include in particular C, the *s*-process elements, as well as He. In stars of extremely low metallicity, dredge-up leads to relevant surface-abundance enhancements for many other species, like O or neutron-heavy species like ^{22}Ne, ^{23}Na, ^{25}Mg or ^{26}Mg.

A very important implication of the third dredge-up is the formation of C stars. Starting on the AGB with a C/O ratio well below unity each third dredge-up mixes a certain amount of mass ($\sim 6 \cdot 10^{-3}$ $M_\odot$ for a core mass of 0.6 $M_\odot$, less for larger core masses) with the intershell-abundance distribution into the envelope. The intershell contains 5 to 10 times more C than O and, as a result, the envelope C/O ratio increases with each dredge-up event until eventually the C/O ratio exceeds unity and a C star is formed.

Dredge-up (DUP) efficiency is expressed by dredge-up parameter $\lambda = \Delta M_{DUP}/ \Delta M_H$, where ΔM_{DUP} is the mass dredged up after a thermal pulse and ΔM_H is the core growth during the preceeding interpulse phase. λ increases with core and

envelope mass and with decreasing metallicity (Lattanzio 1989). Calculations with and without mass loss have been presented by Karakas, Lattanzio & Pols (2002) with the explicit aim of studying how dredge-up depends on mass and metallicity. These calculations show, in agreement with many previous calculations, that the parameter λ reaches very close to unity for intermediate-mass stars. A dredge-up efficiency of $\lambda = 1.0$ implies that the core is not effectively growing.

The luminosity function of C stars, for example in the Magellanic Clouds or in other extra-galactic populations (for example Battinelli & Demers 2004), provide an important tool to test how well the third dredge-up is simulated quantitatively. Such comparisons have been carried out systematically using synthetic evolution models (Section 2.6). Although these models do not contain the input physics that cause the third dredge-up, they can condense the wealth of observational information into easy-to-apply constraints for stellar structure models. Marigo, Girardi & Bressan (1999) found in this way that the third dredge-up should start at a core mass below $0.58\,M_\odot$ with an efficiency of $\lambda = 0.5$.

The reasons why many stellar evolution calculations do not predict sufficiently large dredge-up at sufficiently low core mass (Blöcker 1995; Forestini & Charbonnel 1997; Straniero et al. 1997; Wagenhuber & Groenewegen 1998; Karakas, Lattansio & Pols 2002) and what needs to be improved to reproduce observational constraints has been studied successfully in recent years. A clear link between the adopted physics of mixing and the DUP properties has been established.

As pointed out in Section 2.1 stellar evolution models use the MLT or some variant to describe convective transport. The free mixing-length parameter α_{MLT} specifies the mean free path of a convective blob in units of the pressure scale height H_{P}. In stellar evolution codes this parameter is usually calibrated by matching a $1\,M_\odot$ stellar evolution track at the age of the sun to the solar luminosity and temperature. In most AGB stellar evolution calculations α_{MLT} is kept constant at this solar parameter calibrated value. However, it is not likely that the convection properties of extended giant envelopes, which extend over many pressure scale heights and many hundred solar radii, are well represented by the MLT with a mixing-length parameter appropriate for the sun. Ludwig, Freytag & Steffen (1999) calculated a grid of 2D-radiation hydrodynamic convection models for stellar parameters in the vicinity of the Sun ($4.5 > \log g > 2.5$ and $4500\,\mathrm{K} < T_{\mathrm{eff}} < 7100\,\mathrm{K}$). They determined α_{MLT} from these models and found that stars of solar luminosity $\sim$1500 K cooler are best described by a 15% larger α_{MLT}. These calculations do not extend to the much lower temperatures and much higher luminosities of AGB stars ($\log L/L_\odot \sim 3.5$, $T_{\mathrm{eff}} \sim 2300$ K). They do however reveal a highly nonlinear behavior of α_{MLT} as a function of stellar parameter. This study indicates that the appropriate parameter α_{MLT} for AGB stellar models is uncertain by at least $\pm 20\%$.

The 3D calculations of giant envelopes by Porter & Woodward (2000) span $4.5\,H_{\mathrm{P}}$ and focus on the hydrodynamic properties of envelope convection while simplifying many of the physics components specific to stars. Nevertheless, these simulations show merging downflow lanes that extend over the entire range of

simulation. Further analysis in terms of the MLT as expressed in Cox & Giuli (1968) showed that their simulation for large convective efficiency corresponds to a mixing parameter of $\alpha_{MLT} = 2.68$. Although this value cannot be directly applied to AGB evolution calculations, these and other multidimensional studies of deep-envelope convection support the notion that the very deep-envelope convection of AGB stars may not be accurately described by MLT with a solar-calibrated α_{MLT}. In fact, it may be seriously questioned if the MLT describes AGB envelopes accurately at all, given the vastly different conditions in the highly superadiabatic outer layers and the very efficient adiabatic character of the convection at the bottom in the interior.

Another major difference between the solar convection zone, for which MLT is calibrated and in fact yields satisfactoy results, and the deep stellar envelopes of AGB stars is density contrast, which is orders-of-magnitude larger for AGB envelope convection compared to the sun. This means that the asymmetry between narrow downflows and broad upflows is much larger in AGB stars. Forestini, Arnould & Lumer (1991) accounted for this effect of compressibility by a modified convection theory for stellar evolution that replaces the one mixing-length parameter of MLT by two parameters, one for upflows and one for downflows. In several AGB test evolution models Forestini et al. show that this effect of compressibility acts largely in the same way a larger MLT α-parameter would.

Boothroyd & Sackmann (1988) showed that stellar models with a larger mixing-length parameter predict larger third dredge-up. They find dredge-up in their calculations when the temperature at the bottom of the convective envelope reaches a minimum temperature of $\log T_{CE} = 6.5$ after the thermal pulse. This temperature is reached at lower core and stellar mass in calculations with a larger mixing-length parameter. Marigo, Girardi & Bressan (1999) use this criterion of a maximum temperature reached after the thermal pulse as a free parameter to construct different cases of synthetic AGB models to compare with observational constraints from the C-star luminosity function in the large and small Magellanic Clouds. The description of convection as expressed by the mixing-length parameter used in stellar evolution models is an important component of reproducing the third dredge-up consistent with observations.

Another equally important issue is the physical and numerical treatment of the bottom boundary of the envelope convection as it penetrates (in terms of the Lagrangian mass coordinate) into the H-free core. The situation has been described already by Paczyński (1977). The top layer of the H-free core consists of almost pure helium and the ashes of the H-shell, which has been terminated by the He-shell flash. As the envelope convection bottom approaches the top of the H-free core it encounters first this layer of very low opacity and soon an opacity jump develops. This translates into a jump in the radiative gradient ∇_{rad}. In codes that implement the strict Schwarzschild criterion for convective boundaries this jump becomes an impenetrable barrier for dredge-up (Mowlavi 1999, Herwig 2000). However, a sharp abundance discontinuity at the envelope bottom does not correctly depict the conditions in a real star. The determination of the convective boundary location with

such an abundance discontinuity is unstable as any small amount of mixing across the boundary would relocate it to a lower mass coordinate. There are many physical processes that lead to mixing across the convective boundary even if the boundary location was stable. Mixing processes at this boundary that have been studied in detail include convective overshooting (Herwig et al. 1997, Herwig 2000), rotationally-induced mixing (Langer et al. 1999), and gravity waves (Denissenkov & Tout 2003). In fact, the whole concept of the *s*-process fueled by the ^{13}C neutron source relies on some rather efficient partial-mixing processes across this boundary (Section 3).

There are several approaches for dealing with this convective boundary. One is a largely numerical recipe of premixing one or several radiative grid shells below the convection zone before determining the new convective boundary and repeating this procedure until a stable location for the convective boundary is found (Lattanzio 1989; Frost & Lattanzio 1996; Karakas, Lattanzio & Pols 2002). The problem of the He/H abundance discontinuity is also addressed if either of the above-mentioned physical mixing processes are implemented. This leads to a small layer below the convective region that is partially mixed, and thus erases the abundance discontinuity. In this situation the time step and the grid resolution in the extra-mixing layer are related and care must be taken that the dredge-up is not suppressed by an inappropriate resolution. This has been discussed in detail by Herwig (2000), and it was also shown that within a certain range the actual dredge-up efficiency does not depend on the amount of extra partial mixing. However, if very large overshooting efficiencies are assumed this extra mixing will feed back into the structure and a correlation of dredge-up and overshoot efficiency can then be observed.

Finally, models of the third dredge-up have been calculated using a fully-coupled stellar evolution code (Pols & Tout 2001; Stancliffe, Izzard & Tout 2004b) in which stellar structure, nuclear burning, and chemical mixing are solved simultaneously in each time step (no operator split). An important detail about these calculations is the modification of the MLT-diffusion coefficient at the bottom of the convective envelope. It ensures that the convective-mixing coefficient does not abruptly drop to zero at the convective boundary but decreases gradually to zero inside the convectively unstable zone. This modification was introduced to improve the convergence, but it is inconsistent with a positive superadiabatic gradient $\Delta\nabla > 0$ by definition in the convection zone. Nevertheless, this modification avoids the He/H abundance discontinuity described above, and it is therefore not surprising that Stancliffe, Tout & Pols (2004b) find the third dredge-up with comparable efficiency as do, for example, Karakas et al. (2002) or Mowlavi (1999).

Overcoming the operator split, as done in the Eggleton code (Eggleton 1972) used by Pols & Tout (2001) and Stancliffe, Tout & Pols (2004b) is useful when the characteristic timescale of the operators is comparable and much smaller than the desired numerical time step. This is the case during the actual dredge-up phase for the structure and the mixing operator. In a code that couples these two operators it should be possible to calculate the dredge-up phase with significantly larger

time steps compared to a code with structure-mixing operator split. The fully-coupled code iterates and updates the abundances on both sides of the convective boundary as it simultaneously determines the boundary location. However, there is no principal reason why a calculation with operator split should feature less efficient dredge-up than a code that solves all operators in a coupled manner. In fact, the most recent calculation of initially $2 \, M_\odot$, $Z = 0.01$ thermal pulse AGB (TP-AGB) sequence by Herwig & Austin (2004) using the case with nuclear reaction rates by Angulo et al. (1999), a solar-scaled mixing-length parameter, mass loss, and no overshooting at the bottom of the He-shell flash convection zone shows the first dredge-up on the AGB after the thermal pulse at $M_H = 0.553 \, M_\odot$. Calculations of a $2 \, M_\odot$ model with LMC metallicity of $Z = 0.008$ by Stancliffe, Izzard & Tout (2004a) using the improved Eggleton code (Eggleton 1972) with simultaneous solution of structure find the first third dredge-up after the thermal pulse at core mass $M_H = 0.579 \, M_\odot$. This example supports the assessment that operator split or not should not effect the predicted dredge-up efficiency given that the additional numerical resolution requirements in codes with operator split are appropriately addressed.

In the model by Herwig & Austin (2004), the dredge-up efficiency λ grows almost linear with core mass for a few thermal pulses once the dredge-up has started. However, at a core mass of about $0.58 \, M_\odot$ the dredge-up efficiency peaks at $\lambda \sim 0.3$ and decreases sharply toward the final thermal pulses. This decrease is due to the shrinking envelope mass as the effect of mass loss becomes notable. Stancliffe, Izzard & Tout (2004a) find a maximum $\lambda = 0.88$ for their $2 \, M_\odot$ case, which is probably due to the fact that they have not included mass loss in the stellar evolution calculations.

Beyond the treatment of convective boundaries and the choice of the mixing-length parameter, dredge-up depends on a number of other physics assumptions. Dredge-up predictions depend on nuclear reaction rates. Herwig & Austin (2004) showed that for the range of uncertainties for the important $^{14}N(p, \gamma)^{15}O$ and triple-α reactions given by Angulo et al. (1999), the dredge-up efficiency is uncertain within a factor of two. Considering newer evaluations and experimental data, they adopted a $^{14}N(p, \gamma)^{15}O$ that is almost a factor of two lower than given by Angulo et al. (1999) and found for a $2 \, M_\odot$, $Z = 0.01$ AGB star twice the carbon yields due to doubly-efficient third dredge-up than in the calculation with the Angulo et al. (1999) rate.

The reaction rates have an influence on the dredge-up efficiency because they effect the peak He-shell flash luminosity. Herwig (2000) showed in detail that overshooting at the bottom of the pulse-driven convection zone (PDCZ) increases the third dredge-up efficiency as well. The convective boundary is defined as where the acceleration vanishes ($\Delta \nabla = 0$). There are many studies of stellar convection, both numerical in multidimension as well as analytical, that study the simple fact that because of inertia convective eddies will proceed some finite distance into the stable layer. It is not a question if this overshooting takes place, but only how efficient and far reaching the mixing is that overshooting induces. Numerical

simulations show that in terms of the pressure scale heights overshooting is not equally efficient at the boundaries of different stellar convection zones (Freytag, Ludwig & Steffen 1996; Robinson et al. 2004).

Currently there is no universal theory for overshooting that is applicable to all convective boundaries in stellar evolution. Rather each convective boundary needs to be considered individually. Appropriate ways to determine the mixing efficiency need to be identified. Such mostly semi-empirical methods probe mixing, but cannot distinguish between different causes of mixing, like time- and depth-dependent overshooting, gravity waves, or rotationally-induced mixing. It is then useful to re-interpret the implementation of an exponentially decaying diffusive mixing from the convective region into the neighboring stable layer as representing possibly more than one physical effect acting in similar ways. In Section 3 and 4 some possibilities to constrain the exponential diffusive extra mixing (and other mixing) are described.

Recently the initial C and O abundance in the solar abundance distribution was revised downward (Holweger 2001; Allende Prieto, Lambert & Asplund 2002). Using lower initial C and O abundance would make C-star formation with otherwise identical mixing properties easier, as less nuclear-processed material with C/O > 1 must be mixed into the envelope in order to lift the envelope C/O ratio above unity. However, the new C and O solar abundance come with a grain of salt as solar models using these abundances apparently are in contradiction with critical helioseismological data (Bahcall & Pinsonneault 2004).

Over the past years the understanding of the third dredge-up has significantly improved. The most important ingredients have been identified, and a new attempt including all these issues in one set of calculations should finally resolve the problem of the C-star formation. Such a calculation must take into account the latest simulation results on mass loss of cool giants as well as abundance-dependent molecular opacities (Section 2.1).

2.3. Nucleosynthesis

Nuclear production in AGB stars reflects the coexistence and interplay of the H- and He shells. It is dominated by the complex cycles of convective mixing and the periodically changing thermodynamic conditions induced by the recurrent flash-burning events in the He shell (Figure 3). Nuclear production in AGB stars is important for the chemical evolution of galaxies because of their capability to produce an array of elements just from helium and hydrogen. This primary production includes important elements like carbon and nitrogen, as well as neutron-heavy species like ^{22}Ne. Other neutron-heavy species like ^{25}Mg and ^{26}Mg have both a primary as well as a secondary component, and which one dominates depends on the metallicity.

The peculiar property of AGB stars that make their nucleosynthesis so interesting (but also complicated) is their ability to expose nuclei to H burning and He burning, and H burning again, then possibly to He burning and the high neutron

fluxes in the He-burning shell again, and finally to eject the material through high mass-loss rates.

The way nuclei are made is increasingly interesting for higher mass numbers. Carbon is generated from triple-α reactions in the He shell. The triple-α reaction provides energy almost exclusively during the He-shell flash. Oxygen is produced significantly only in the deeper radiative parts of the He shell. The amount of oxygen that can be found in the PDCZ depends on exponential overshooting (or similar processes, see Section 2.2), and this is discussed in Section 3. After the He-shell flash the third dredge-up may occur and the primary C and O is mixed into the envelope.

When the H shell resumes, it processes H-rich envelope material. As it burns outward it leaves behind H-burning ashes: He and CNO in the CNO-cycle equilibrium ratios. Thus, in the H-shell ashes almost all C and O is transformed into ^{14}N. This ^{14}N is primary and the result of consecutive He and H burning. In low-mass AGB stars, primary ^{14}N is not in the envelope but below the H shell. Only massive AGB stars that reach high enough temperatures at the bottom of the envelope convection produce ^{14}N in the envelope (Section 2.5). The ^{14}N in the H-burning ashes below the H shell is different from the ^{14}N in the ^{14}N pocket described in Section 3. The ^{14}N pocket is the result of an additional partial mixing process that is primarily required to generate a ^{13}C pocket.

The order of magnitude of ^{14}N in the H-shell ashes that will be ingested into the next PDCZ can be easily estimated. The typical dredged-up mass for a low-mass AGB star is $\Delta M_{\text{DUP}} \sim 5 \cdot 10^{-3} \, M_\odot$ per thermal pulse, where $\Delta M_{\text{DUP}} = M_{\text{HTP}} - M_{\text{HDUP}}$, M_{HTP} is the H-free core mass at the thermal pulse, and M_{HDUP} is the minimum mass of the bottom of the envelope convection reached during the dredge-up. Assuming a mass fraction of $X(\text{C} + \text{O})_{\text{PDCZ}} = 0.5$[1] in the PDCZ and an envelope mass of $M_{\text{env}} = 1 \, M_\odot$, the mass fraction of C + O will increase by $\Delta X(\text{C} + \text{O})_{\text{env}} = \Delta M_{\text{DUP}} \cdot X(\text{C} + \text{O})_{\text{PDCZ}}/M_{\text{env}} = 2.5 \cdot 10^{-3} \, M_\odot$. An AGB star of the LMC with $Z = 0.008$ may have an initial C and O mass fraction abundance of $1.2 \cdot 10^{-3}$ and $3.8 \cdot 10^{-3}$, respectively. Thus, after four thermal pulses with dredge-up one may expect $X(\text{C} + \text{O})_{\text{env}} = 1.5 \times 10^{-2}$. If the dredge-up parameter in our example was $\lambda = 0.5$ and if this efficiency is assumed constant over a few thermal pulses, then the H shell burns outward through $\Delta M_{\text{H}} = \Delta M_{\text{DUP}}/\lambda = 2 \cdot \Delta M_{\text{DUP}} = 10^{-2} \, M_\odot$ before the next He flash develops. Its convection zone will therefore engulf $M_{\text{N14}} \sim X(\text{C} + \text{O})_{\text{env}} \cdot \Delta M_{\text{H}} = 1.5 \times 10^{-4} \, M_\odot$.

The PDCZ itself has a typical mass of $M_{\text{PDCZ}} \sim 1.5 \cdot 10^{-2} \, M_\odot$ and all ^{14}N is transformed by α captures, first into ^{18}O and then into ^{22}Ne. Thus the ^{20}Ne abundance in the PDCZ will be of the order $X(^{22}\text{Ne}) \sim (22/14) \cdot (M_{\text{N14}}/M_{\text{PDCZ}}) \sim 10^{-2}$. In low-mass AGB stars the temperature at the bottom of the PDCZ is not high enough to burn more than a few percent of ^{22}Ne via the α-capture reactions

---

[1]This C and O abundance in the PDCZ is typical for models in which some overshooting at the bottom of this convection zone is assumed (cf. Section 4.2). For models without overshooting this value is $\sim$0.25.

^{22}Ne(α, n)^{25}Mg and ^{22}Ne(α, γ)^{26}Mg, and the neon abundance will accumulate over all thermal pulses to reach approximately 2% by mass. This neon abundance in the intershell can be verified observationally as described in Section 4. This primary neon is the result of four distinct consecutive burning phases of H and He. In extremely metal-poor stars (Section 6), if either a neutron from ^{22}Ne(α, n)^{25}Mg or a proton during hot-bottom burning is added to ^{22}Ne the AGB star produces primary ^{23}Na (Herwig 2004c).

In addition to the primary production, AGB stars host the secondary production of a number of elements. The radioactive ^{26}Al (ground-state: $t_{1/2} = 7.6 \times 10^5$ yr) is of particular interest because of its relevance to gamma-ray astronomy and for the interpretation of presolar grains (Forestini, Arnould & Paulus 1991; Mowlavi & Meynet 2000). ^{26}Al is made in H-shell burning during the interpulse in the MgAl cycle. It enters the PDCZ with the other H-shell burning ashes when the next He-shell flash emerges (Figure 3). Here ^{26}Al is partly destroyed by exposure to neutrons.

AGB production plays an important role in the galactic chemical evolution of flourine (Renda et al. 2004). The nucleosynthesis of F in AGB stars is intimately related to the *s* process because the reaction chain to ^{19}F in any case involves He burning and goes through the neutron-heavy nitrogen istope. In He burning the proton required for making ^{15}N can only come from an (n, p) reaction, in particular the ^{14}N(n, p)^{14}C. The neutrons for this reaction chain are the same as for the *s* process and generated under radiative conditions in the ^{13}C pocket in the interpulse phase. Observations have revealed a trend between F and C (Jorissen, Smith & Lambert 1992), as predicted by theory. AGB models currently do not reproduce the observed F-C relation quantitatively (Forestini et al. 1992; Mowlavi, Jorissen & Arnould 1996; Karakas & Lattanzio 2003; Lugaro et al. 2004). As discussed in Section 4.2 the problem may be related to missing physics in the AGB models.

2.4. The Evolution of C and O

The evolution of C and O in AGB stars depends on many aspects, like mass loss and opacities (Section 2.1), the third dredge-up (Section 2.2), and nucleosynthesis (Section 2.3). Observables are the stellar C and O abundances of AGB stars, the luminosity function, and the number ratios of C-rich and O-rich stars in extragalactic populations. In particular the Magellanic Clouds have been explored extensively in comparison with parameterized synthetic AGB models (Section 2.6) in order to determine the quantitative third dredge-up properties that evolutionary AGB models are required to reproduce.

The elemental C and O abundances of AGB stars and of planetary nebulae are shown in Figure 6 together with models. A simple parameterized synthetic mixing model starts with an envelope of given mass and initial abundance and calculates the envelope enrichment with C and O for average values of mass loss, dredged-up mass per pulse, intershell abundance, and interpulse time. The purpose of this synthetic model is to demonstrate some basic properties of low-mass AGB stars.
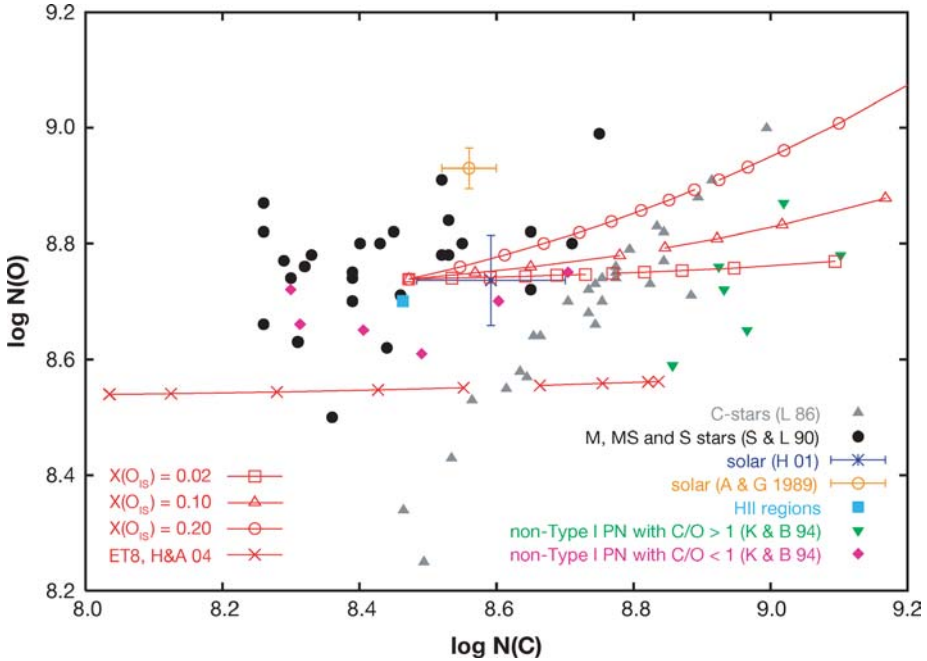
Figure 6 Carbon and oxygen abundances (*number fractions*) of AGB stars. The simplified C and O mixing model (*open symbols*) assumes an envelope mass of $1.6\,M_\odot$ when the dredge-up starts and an initial solar envelope abundance of C and O according to Holweger (2001), approximately corrected for the carbon-depleting effect of the first dredge-up. A constant dredged-up mass at each thermal pulse of $2.5 \cdot 10^{-3}\,M_\odot$ corresponding to a dredge-up parameter of $\lambda \sim 0.5$, an intershell period of 10^5 yr, and a constant mass-loss rate of $3 \cdot 10^{-7}\,M_\odot$/yr for C/O < 1 and $3 \cdot 10^{-6}\,M_\odot$/yr for C/O > 1 has been assumed. The three cases are for different intershell abundances of O, as given in the legend. The lowest oxygen intershell abundance corresponds to an evolution calculation without overshooting. The fourth model is the detailed stellar-evolution sequence ET8 of Herwig & Austin (2004) with Z = 0.01. The break in the *red solid lines* separates the O-rich and the C-rich part of the tracks. Observational data are from Lambert et al. (1986), Smith & Lambert (1990), Anders & Grevesse (1989), and Kingsburgh & Barlow (1994).

In addition the model can clarify the effect of the O abundance in the intershell on overabundances in the envelope, and how this compares to observations.

The model ET8 (Figure 6) is a detailed stellar evolution model. Mass loss has been considered according to the formula derived by Blöcker (1995) as a fit to the pulsating wind models of Bowen (1988). Although pulsating wind models are being constantly improved (Section 2.1) the latest results have not yet entered the routine stellar evolution modeling of AGB stars. Model ET8 has been computed without overshooting at the bottom of the PDCZ. In models without overshooting,

the mass fraction of ^{16}O is 2% in the PDCZ (Schönberner 1979). Model ET8 corresponds to the mixing model with $X(O_{IS}) = 0.02$ (*open squares*). In both cases the third dredge-up brings intershell material to the surface that contains about 20% C and 2% O, leading to a horizontal evolution in Figure 6 from left to right.

Models with overshooting that agree with the observational constraints from H-deficient post-AGB stars (Section 4.2) have a PDCZ abundance of $\sim 8 \cdots 15\%$ ^{16}O (Herwig 2000). In the solar distribution oxygen is 1% by mass (Anders & Grevesse 1989).[2] Therefore, admixture of intershell material that is barely more abundant in O than the envelope material will not change the observable abundance significantly. Even an abundance of 10% oxygen in the dredged-up material would be barely observable in AGB stars. This is demonstrated by the mixing models with enhanced O intershell abundance (Figure 6). The presence of a small amount of overshoot at the bottom of the PDCZ leading to an intershell abundance of 10% O can not be distinguished from a case without PDCZ overshooting. It seems that the case with 20% O intershell abundance is not consistent with the present data.

Finally, Figure 6 shows again that a rather short lifetime of C-rich AGB stars with only a couple thermal pulses is consistent with observational data. Otherwise, if many thermal pulses follow the C-star formation, planetary nebulae should cover a range to much larger C abundances. C stars have larger mass loss than O-rich stars of the same initial mass and metallicity because their luminosity is higher. In addition, the different molecular composition of a C-star atmosphere compared to the O-rich atmosphere leads to lower stellar temperature and higher mass loss (Section 2.1).

2.5. Hot-Bottom Burning

Massive AGB stars are characterized by hot-bottom burning (HBB), a colorful name for a H-shell burning condition in which the outer part of the shell is included in the envelope convection. The H shell has enhanced access to fuel, convectively mixed into its outer layers. This leads to an overluminosity of massive AGB stars compared to the core-mass luminosity relation derived from evolution calculations of low-mass AGB stars (Blöcker & Schönberner 1991). For larger core as well as envelope mass a larger fraction of the H shell is included in the convection zone and hot-bottom burning is more efficient. This means that the temperature at the bottom of the convective envelope is larger.

Hot-bottom burning transforms dredged-up C efficiently into N, which initially prevents C-star formation (Boothroyd, Sackmann & Ahern 1993). However, at the end of the AGB evolution mass loss has reduced the envelope mass and hot-bottom burning becomes less efficient. According to Frost et al. (1998) C dredge-up

---

[2]The effect of the recently revised solar O and C abundance has been addressed in Section 2.1.

can be more efficient than hot-bottom burning in intermediate-mass stars with only a small envelope left. This leads to the formation of the most luminous C stars.

For a given initial mass the core mass of an AGB star is larger for lower metallicity. Thus, the lower initial-mass boundary for hot-bottom burning decreases with lower metallicity. Forestini & Charbonnel (1997) find hot-bottom burning for $M_{ini} \geq 5\,M_\odot$ for $Z = 0.02$, whereas at $Z = 0$ hot-bottom burning is found down to $3\,M_\odot$ (Siess, Livio & Lattanzio 2002). The nucleosynthesis signature of hot-bottom burning includes Li production, a high He and N abundance, a low C/O and $^{12}C/^{13}C$ ratio, as well as enhancements of ^{23}Na, ^{25}Mg, ^{26}Mg and ^{26}Al (Sackmann & Boothroyd 1992; Boothroyd, Sackmann & Wasserburg 1994; Forestini & Charbonnel 1997; Ventura, D'Antona & Mazzitelli 2002; Karakas & Lattanzio 2003; Denissenkov & Herwig 2003). Hot-bottom burning may play a particularly important role at extremely low metallicity (Section 6.3) and in super-AGB stars (Section 5).

Quantitative hot-bottom burning predictions depend (like the dredge-up results) on the adopted mass loss and on the theory of convection. In the framework of the MLT hot-bottom burning is more efficient for a larger MLT parameter α_{MLT}. The full-spectrum theory replaces the mixing-length picture of one convective bubble by a spectrum of bubble sizes that aim to better represent the range of scales in turbulent convection. This convection theory predicts generally more efficient convection than MLT. For a given mass and metallicity hot-bottom burning is more efficient with the full-spectrum theory compared to the mixing-length case (Mazzitelli, D'Antona & Ventura 1999, Ventura & D'Antona 2005). Other properties of convective AGB envelopes, as for example compressibility accounted for by Forestini, Arnoul & Lumer (1991), may also increase HBB efficiency (Section 2.2).

2.6. Synthetic AGB Models and Postprocessing

Postprocessing models take the detailed thermodynamic information from stellar structure calculations as input for single- or multizone nucleosynthesis calculations. This approach is useful to study complex schemes of nucleosynthesis in which the effect of different sets of nuclear input physics needs to be evaluated. For example, Lugaro et al. (2004) studied how the still uncertain ^{19}F synthesis in AGB stars depends on the nuclear physics input. For some applications the mixing processes included in stellar evolution calculations are insufficient or uncertain. Postprocessing models allow study of parameterized mixing. Currently, the *s* process in AGB stars is quantitatively calculated using this approach (Section 3.1).

Synthetic AGB models use a set of fitting formulae to properties of evolution models, thereby parameterizing the properties of AGB stars (Marigo, Chessan & Chiosi 1996). Contrarily, stellar-evolution models' often parameterize physical processes. In some cases synthetic models can reproduce observations quantitatively better, because they can be calibrated well with observations. However,

synthetic models cannot be extrapolated into regimes that have not yet been explored in detail with stellar evolution models. Therefore the synthetic modeling approach is currently not applicable to extremely low or zero metallicity. Despite these disadvantages synthetic models have one big advantage—speed. Large and high-resolution grids of rather detailed yield predictions are available through this method (Marigo 2001). The calibration of the synthetic models involves matching many observables, including the C-star luminosity function in the Magellanic Clouds or the white dwarf mass distribution. This has lead to much better quantitative characterization of dredge-up in AGB stars (Marigo, Girardi & Bressan 1999). Some synthetic models now include an envelope integration that allows calculation of the hot-bottom burning phase of massive AGB stars (Marigo 1998; Marigo, Bressan & Chiosi 1998). Other sets of synthetic models have been constructed with specific applications in mind, including synthetic binary models (Izzard et al. 2004) or old- and intermediate-age populations as tools to study extra-galactic systems (Mouhcine & Lançon 2002).

3. THE *s* PROCESS

The *s* process is the origin of half of all elements heavier than iron (Arlandini et al. 1999). It is also important for isotopic ratios and in some cases elemental abundances of lighter elements particularly at extremely low metallicity. The heavy elements are made by the *s* process through neutron captures that are slow compared to the competing β-decay. Starting from the abundant iron group elements it follows closely the valley of stability in the chart of isotopes. It is characterized by neutron densities $N_n < 10^{11}$ cm^{-3}. Observations and theory agree that the nuclear production site of the main and strong component of the *s* process ($90 < A < 204$) originates in low-mass AGB stars. The weak component below the first *s*-process peak at $A = 90$ is produced during He and C burning in massive stars. Here we deal only with the *s*-process in AGB stars.

The *s* process in low-mass AGB stars has two neutron sources. The main source is ^{13}C, which forms via the ^{12}C(p, γ)^{13}N(β^+)^{13}C reaction. At the end of the dredge-up phase (Section 2.2, Figure 3) after the He-shell flash, when the bottom of the H-rich convective envelope has penetrated into the ^{12}C-rich intershell layer, partial mixing at this interface would create a thin layer providing simultaneously the required protons and ^{12}C. The *s* process in the ^{13}C pocket is characterized by low neutron densities (log $N_n \sim 7$) that last for several thousand years under radiative, convectively stable conditions during the quiescent interpulse phase. The physics of mixing at the H/^{12}C interface at the end of the third dredge-up phase has not yet been clearly identified (see below). Most likely it is some type of convection-induced mixing beyond the convection boundary.

The ^{22}Ne(α, n)^{25}Mg reaction requires the high temperatures that can be found at the bottom of the PDCZ during the He-shell flash ($T > 2.5 \cdot 10^8$ K). The neutrons are released with high density (log $N_n \sim 9 \ldots 11$) in a short burst (Gallino et al. 1998). These peak neutron densities are realized for only about a year, followed

by a neutron-density tail that lasts a few years, depending on the stellar model assumptions.

3.1. The Postprocessing Parameterized s-Process Model

The theoretical description of the s process has undergone a remarkable evolution. Starting from semi-analytical models of an exponential superposition of neutron exposures, it has in recent years developed to the detailed postprocessing models with a strong tie to realistic models of the actual time-dependent thermodynamic condition of the nuclear production site in the stellar interior. This evolution and the properties of the current state-of-the-art models are covered in depth in the review paper by Busso, Gallino & Wasserburg (1999). The basic idea of the new s-process models is to use the thermodynamic output from a stellar-evolution calculation including mass loss as input for nucleosynthesis calculations with a complete s-process network. This postprocessing step involves the thermodynamic trajectories of the stellar interior that contain the neutron-rich conditions. In this approach the thermodynamic conditions according to the stellar-evolution calculation are considered as a fixed background. No feedback of the assumed mixing processes into the stellar structure is allowed. The postprocessing accounts for both the ^{13}C neutron source as well as for the ^{22}Ne source, and mixes the different contributions according to the information provided by the stellar-evolution calculations. The model has one free parameter, which is the ^{13}C abundance in the ^{13}C pocket. This accomodates for the fact that mixing processes, which are responsible for bringing protons down from the envelope into the ^{12}C-rich core to enable ^{13}C formation, are not explicitly included in this model.

The neutron exposure $\tau = \int N_{\rm n} v_{\rm T} dt$, where $N_{\rm n}$ is the neutron density and $v_{\rm T}$ is the thermal velocity, is proportional to the amount of ^{13}C in the pocket. In the present paradigm, the bulk of the trans-iron s-process nuclei are formed in the ^{13}C pocket. A larger neutron exposure will in general lead to a distribution containing more species at the higher mass s-process abundance peak ($A \sim 140$) including Ba, La, Ce, Nd, and Sm compared to the abundances at the first s-process peak ($A \sim 90$) including Y, Sr, and Zr. Observers average the abundances of the first group as the heavy s-process index hs and the second as the light s-process index ls. The hs/ls ratio in s-process models with higher ^{13}C abundance in the ^{13}C-pocket is higher. However, as the neutron exposure increases above $\sim$1 mbarn (at 8 keV) all the flux goes to produce Pb and the hs/ls ratio decreases again to a value around 0.6 dex. Moreover, the predicted hs/ls values are a function of the metallicity. The ^{13}C in the ^{13}C pocket is proportional to the ^{12}C abundance in the PDCZ, which is primary. As the abundance of s-process seed material and neutron poison decreases with metallicity the neutron exposure increases, and therefore the maximum hs/ls values are reached at lower metallicities (Busso et al. 2001). All these effects are now taken into account quantitatively in models of the galactic chemical evolution of the heavy elements (Travaglio et al. 2001, 2004).

Observations of the hs/ls ratio for a range of metallicities and different classes of objects reveal an important property of the s process, which has yet to be explained.

Stars of the same mass and metallicity seem to display a spread of hs/ls ratios that must somehow correspond to a range of conditions in otherwise rather similar stars (Nicolussi et al. 1998, van Winckel & Reyniers 2000, Busso et al. 2001, van Eck et al. 2003). SiC grain data indicate that a spread by a factor of five is necessary for the neutron exposure for a given mass and metallicity (Lugaro et al. 2003a). This spread is accounted for by a range of different cases in which each of the ^{13}C abundance in the pocket is assumed to be different (Busso et al. 2001).

The mass of the ^{13}C pocket is mainly responsible for obtaining the overall overabundance, but it has only a small effect on the abundance distribution. Therefore the ^{13}C-pocket mass can be determined independently from the neutron exposure in the pocket. Herwig, Langer & Lugaro (2003) derived the basic properties of the ^{13}C pocket in a semi-analytical way, and their results are in agreement with more detailed numerical models. Accordingly, the ^{13}C pocket should generate a neutron exposure in the range of 0.2–0.5 mbarn^{-1} and the mass layer ΔM_{spr}, in which s-process material has actually formed owing to the presence of additional ^{13}C, is $\Delta M_{\mathrm{spr}} > 7 \cdot 10^{-5} \, M_{\odot}$.

The parameterized, postprocessing s-process model (Busso, Gallino & Wasserburg 1999) has made it possible to relate the accurate isotopic measurements from presolar meteoritic SiC grains and individual stellar abundance observations, as well as the galactic chemical evolution of s-process-dominated elements to physical processes inside stars. Based on this important step forward one may now use the s process to learn more about the details of mixing inside AGB stars (Section 3.3). Whatever one can learn about physical processes inducing mixing consistent with the s process in AGB stars is relevant for stars of all masses, and therefore the s process in AGB stars is an important tool to learn more about the evolution of stars in general.

3.2. Mixing for the s Process

The first important question is what physical processes are responsible for the mixing of protons and ^{12}C at the end of the third dredge-up when the base of the envelope has reached its lowest mass coordinate. Currently, there are three processes proposed in the literature. The first is exponential diffusive overshooting (Herwig et al. 1997; Herwig 2000), the second is mixing induced by rotation (Langer et al. 1999), and the third is mixing by internal gravity waves (Denissenkov & Tout 2003). Each of these effectively leads to a continuously and quickly decreasing mixing efficiency from the H-rich convection zone into the radiative ^{12}C-rich layer. As for any mixing process that causes a continuous decrease of the H/^{12}C ratio below the convective boundary these processes will lead to the formation of two pockets, a ^{13}C and a ^{14}N pocket, that are overlapping (Lugaro et al. 2003b). At low H/^{12}C ratios H burning is proton limited. In this regime the few available protons will make first ^{13}C via the ^{12}C(p, γ) reaction but the ^{13}C does not reach high enough values to compete with ^{12}C for protons. Thus, in this lower layer of the partial mixing zone, only ^{13}C forms and ^{14}N does not. However at somewhat

larger mass coordinates where the H/^{12}C ratio is initially high enough, protons are available after the first ^{13}C forms and soon this ^{13}C competes effectively with ^{12}C for protons. In the end a ^{14}N pocket forms with a maximum abundance that only depends on the initial ^{12}C abundance in the intershell. Equally, the maximum ^{13}C abundance in the ^{13}C pocket depends linearly on the intershell ^{12}C abundance obtained during the He-shell flash in the PDCZ. Therefore, the conditions in the ^{13}C pocket are not independent of the mixing at the bottom of the PDCZ. As shown by Lugaro et al. (2003b), the neutron exposure in the ^{13}C pocket is proportional to the ^{12}C abundance in the PDCZ, which depends on the amount of overshoot or other convective extra mixing, like the gravity waves proposed by Denissenkov & Tout (2002). Lugaro et al. (2003b) derive the relationship $\tau_{\max} = 1.2X(^{12}\text{C})_{\text{IS}} + 0.4$, where $X(^{12}\text{C})_{\text{IS}}$ is the intershell ^{12}C-mass fraction and $\tau_{\max}$ is the maximum neutron exposure reached in the ^{13}C pocket. In Section 4, observations are described that can directly verify the C content of the PDCZ.

The three processes for creating a ^{13}C pocket are very similar in that they all predict a ^{14}N and a ^{13}C pocket. For the same ^{12}C abundance in the intershell the maximum neutron exposure in the pocket is about the same in all three cases. The next issue is the mass ΔM_{spr}, which eventually contains s-process enriched material. In the exponential overshooting model, the mixing coefficient is written as $D_{\text{OV}} = D_0 \exp(\frac{-2z}{f_{\text{ov}} \cdot H_{\text{p}}})$, where D_0 is the MLT mixing coefficient at the base of the convection zone, z is the geometric distance to the convective boundary, H_{p} is the pressure scale height at the convective boundary, and f_{ov} is the overshooting parameter. If applied to core convection, $f_{\text{ov}} = 0.016$ reproduces the observed width of the main sequence (Herwig et al. 1997). A similar overshooting model was, for example, used by Ventura et al. (1998).

The AGB models with overshooting used this value initally at all convective boundaries, resulting in a ^{13}C pocket that was at least one order of magnitude too small in mass (Herwig 2000). Lugaro et al. (2003b) studied the effect of different stellar evolution input on s-process predictions. In the course of this study $f_{\text{ov}} = 0.128$ was used at the bottom of the convective envelope and generated a large enough ^{13}C pocket. However, the maximum neutron exposure in the ^{13}C pocket of the overshooting model is $0.7 \cdots 0.8 \, \text{mbarn}^{-1}$, whereas in the non-overshooting models this value is $0.4 \, \text{mbarn}^{-1}$. It should be mentioned again, that in the nonovershooting models, the amount of ^{13}C, and thus the maximum neutron exposure, in the ^{13}C pocket is fitted to the observations. Correspondingly, Lugaro et al. (2003b) obtained only negative values for the logarithmic ratio [hs/ls], whereas the overshooting model with the larger neutron exposure predicts [hs/ls] ~ 0 for the nonovershooting models. This compares to an observed range of $-0.6 < [hs/ls] < 0.0$ for stars of solar metallicity (see Busso et al. 2001, for a compilation of observational data). Thus, it seems that the overshooting models can reproduce only the largest observed hs/ls ratios, indicating that the neutron exposure in the ^{13}C pocket in these models is at the maximum of the observationally bounded range.

However, as explained above, the larger neutron exposure in the overshooting models is not the result of the way the partial-mixing region forms at the end of the

third dredge-up, but it is due to the larger C abundance that models with overshooting generate in the PDCZ. If one would construct a model with overshooting only at the bottom of the envelope convection, the resulting neutron exposure would very well agree with the neutron exposure assumed in models with parameterized ^{13}C pocket, which successfully reproduce the average of the observed hs/ls ratios.

This, however, is not the correct solution. First, this would not be in agreement with the constraints on the intershell C abundance presented in Section 4. In addition, it would not allow for reproducing those observations that, in fact, do require a larger neutron exposure in the ^{13}C pocket ([hs/ls] $\sim$ 0), and it does not provide for a mechanism to account for the observed spread of neutron exposure. In fact, the intershell ^{12}C abundance is the only way to increase the neutron exposure significantly above the peak value of 0.35 mbarn^{-1} corresponding to an intershell ^{12}C abundance of 0.2. However, we do not have any reason to change the ^{12}C intershell abundance in a random way within a factor of five from one star to another with otherwise identical parameters. Besides, this is not supported by observations described in Section 4.

In an attempt to find solutions to these problems Herwig & Langer (2001b) started to analyze the *s*-process properties of AGB stellar models with rotation in more detail. The first finding was that, with the unmodified set of parameters contained in the rotation implementation that had been used previously for calculations of rotating massive stars (Heger, Langer & Woosely 2000), the ^{13}C pocket generated by shear mixing below the envelope convection base was about an order of magnitude smaller than what is needed in the partial-mixing zone of a nonrotating model to reproduce the observed *s*-process elements in stars. The second important finding was that shear mixing, which initially generates the ^{13}C pocket, prevails throughout the interpulse phase, even when the base of the convection is receding in mass after H-shell burning has resumed. When the dredge-up ends, the low-density, slowly rotating convective envelope and the fast-rotating compact radiative core are in contact, and mixing is induced through shear at this location of large differential rotation. This radial velocity gradient remains as a source for shear mixing at exactly the mass coordinate of the ^{13}C pocket with important consequences for the *s*-process. Shear mixing during the interpulse phase swamps the ^{13}C pocket with ^{14}N from the pocket just above. By the time the temperature has reached about $9 \cdot 10^{7}$ K and ^{13}C starts to release neutrons via ^{13}C(α, n)^{16}O, ^{14}N is, in fact, more abundant than ^{13}C in all layers of the ^{13}C pocket. ^{14}N is a very efficient neutron poison. It has a very large ^{14}N(n, p)^{14}C rate and simply steals neutrons from the iron seed. As a result, the neutron exposure is only $\sim$0.04 mbarn^{-1}, about a factor of 10 too small to generate the observed *s*-process abundance distribution (Herwig, Langer & Lugaro 2003; Siess, Goriely & Langer 2004). The detailed postprocessing models of current rotating AGB stars showed that they are not capable of accounting for the observed *s*-process overabundances.

Although none of the concepts discussed so far appear to solve the mixing problem for the *s*-process by itself, a combination of them leads to a solution. Let's examine first a model that includes convection-induced, exponentially decaying extra mixing at all convective boundaries. The overshooting efficiency at the

bottom of the PDCZ is chosen so that the ^{12}C mass fraction is about 0.45, roughly twice the value found in models without overshooting at the bottom of the PDCZ. Such an overshooting value would be in the range $f_{PDCZ} = 0.005\dots0.015$. The overshooting efficiency at the bottom of the convective envelope is chosen large enough to make a broad enough pocket ($f_{CE} \sim 0.13$) to explain the observed overabundances. This combination would lead to a sufficient amount of s-process production, but the heavy s-process elements at the second peak would be too abundant for most observed stars, because the neutron exposure is too large. The ^{12}C intershell abundance and, therefore, the ^{13}C abundance in the pocket and thus the neutron exposure are twice the values as in models without PDCZ overshooting. This combination can however reproduce the largest logarithmic [hs/ls] ratios of zero at solar metallicity (Lugaro et al. 2003b).

We then add rotation to this picture. Possibly shear mixing has not the decisive effect on the initial creation of the ^{13}C pocket. But the admixture of ^{14}N during the interpulse phase would, in fact, lead to a reduction of the neutron exposure. By starting with an upper limit of the neutron exposure as a result of overshooting from the PDCZ, an effect to lower that maximum neutron exposure preferentially in a random way is in fact needed. ^{14}N poisoning may be the answer! The models with rotationally-induced mixing predict mixing coefficients of the order log $D_{rot}(cm^2/s^{-1}) \sim 2$ and, as mentioned earlier, lead to neutron exposures of $\tau \sim 0.04$ mbarn^{-1}. Herwig, Langer & Lugaro (2003) have constructed a set of synthetic models in order to find the order of magnitude for the interpulse mixing between the ^{14}N and ^{13}C pockets that would cover the observed spread in neutron exposures. They found that $0.0 > \log D_{IP}(cm^2/s^{-1}) > -2.0$ correspond to a range of neutron exposures $0.12 < \tau(mbarn^{-1}) < 0.64$, which should roughly cover the observed spread of hs/ls ratios. In this picture of mixing for the s process many pieces fall nicely into place. The larger ^{12}C abundance in the intershell, which is desired to explain observations described in Section 4.2, and which has caused problems by causing too large neutron exposures in the ^{13}C pocket, is now actually necessary. It lifts the neutron exposure to a maximum required value, from which admixture of poison can generate a distribution of hs/ls predictions.

The remaining problem in this picture is to explain the magnitude of mixing necessary to make the scheme work. It seems that rotation implies too much mixing. Magnetic fields may add coupling between the fast rotating core and the slowly rotating envelope and provide additional angular momentum transport. That could lower the angular velocity gradient at the core–envelope boundary where the ^{13}C pocket forms and reduce mixing between the ^{13}C and ^{14}N pocket. It is interesting to note that such an effect of magnetic fields may also help to reconcile the predicted rotation rates of AGB cores of ~ 30 km/s with the rotation rate determinations of white dwarfs. Spectroscopic determinations of rotation rates of white dwarfs of spectral type DA cannot rule out such values, but most are also consistent with zero or very low rotation (Koester et al. 1998; Heber, Napiwotzki & Reid 1997). However, asteroseismological measurements of white dwarf (WD) rotation rates clearly yield such smaller values in the range of $0.1 < v_{rot}/(km/s) < 1$ (see references in Kawaler 2003).

3.3. *s* Process as a Diagnostic Tool

The previous section described mixing processes on a level of accuracy that corresponds to the global properties of the *s* process, the ratio of the heavy-to-light peak elements, and the overall overproduction of the *s*-process elements. In addition, the high-precision information on the presolar meteoritic SiC grains provide isotope ratio measurements that allow probing the conditions at the *s*-process nuclear production site in more detail. One example is the highly temperature-dependent nucleosynthesis triggered by the release of neutrons from ^{22}Ne at the bottom of the PDCZ.

Stellar evolution models show that the temperature at the bottom of the PDCZ correlates with the efficiency of extra mixing like overshooting at the bottom of this convection zone (Herwig 2000). Neutrons in the PDCZ are generated by the ^{22}Ne$(\alpha, n)^{25}$Mg reaction. For larger temperatures the neutron density is higher. Isotopic ratios that enclose a branch point isotope in the *s*-process path will be more neutron heavy for higher neutron densities. An example is the ^{96}Zr/^{94}Zr-ratio. Figure 7 shows the situation in the chart of isotopes. The main flux of neutron captures in the *s* process follows the path given by the *thick red line*. The half-life of ^{93}Zr is much longer than the neutron-capture timescale. This is not the case for ^{95}Zr with a β-decay half-life of 64d. For low-neutron densities, ^{95}Zr decays. For $N_n > 3 \cdot 10^8$ cm^{-3} ^{95}Zr$(n, \gamma)^{96}$Zr becomes significant, hence ^{96}Zr is produced. If the temperature is larger, the neutron density is larger and the ^{96}Zr/^{94}Zr ratio, which can be measured in SiC grains, is larger as well.

Lugaro et al. (2003a) studied the measured isotopic ratios of Mo and Zr as well as Sr and Ba from SiC grains in the context of the postprocessing model described in Section 3.1. They evaluate the sensitivity of their results in terms of nuclear reaction rate uncertainties. All branchings activated by the ^{22}Ne neutron source
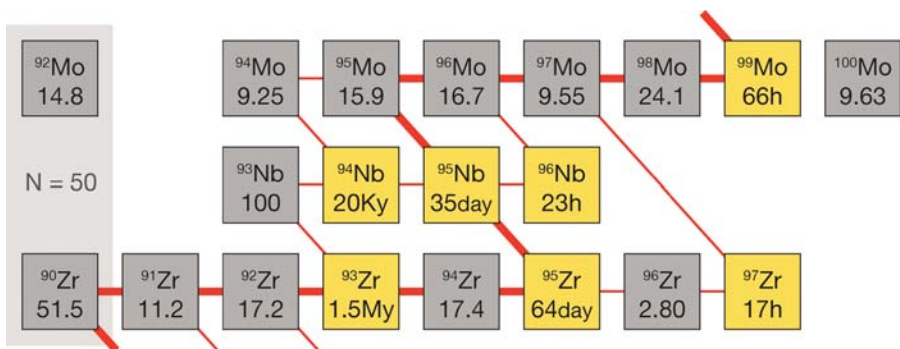
Figure 7 Detail of the chart of isotopes from zirconium to molybdenum. Unstable isotopes are represented in yellow. The *thicker red line* shows the main path of the *s* process; the *thinner red line* shows generally less important side branches. The additional numbers in the boxes give the half-life of unstable isotopes and the isotopic abundance fraction for the stable isotopes.

depend on the still uncertain $^{22}Ne(\alpha, n)^{25}Mg$ rate. In addition, the $^{96}Zr/^{94}Zr$ ratio depends on the neutron cross section of the unstable isotope ^{95}Zr. As for almost all radioactive nuclei the (n, γ) rate of ^{95}Zr is not measured. The theoretical estimates vary from Maxwellian-averaged cross sections of 20 mb (Beer, Voss & Winters 1992) to 140 mb (JENDL-3.2).

Beyond the nuclear reaction rate uncertainties, Lugaro et al. (2003a) study the dependence of the isotopic ratio predictions to the neutron exposure of the parameterized postprocessing model (Section 3.1) in the radiative intershell s-process production site fueled by ^{13}C. As explained in Section 3.2, the ^{13}C abundance in the ^{13}C pocket depends on the ^{12}C abundance in the PDCZ. Current models indicate that a variation of the ^{12}C abundance through mixing processes at the bottom of the PDCZ is correlated with the temperature for the ^{22}Ne neutron source at the bottom of the PDCZ. Goriely & Mowlavi (2000) showed that the s-process abundance distribution, and therefore the neutron exposure in the ^{13}C pocket is independent of the functional form of the proton profile reaching into the ^{12}C-rich core. The idea here is that maybe different physical mixing processes would lead to different profiles that would then be distinguishable through their s-process signature. However, as already mentioned in Section 3.2, the maximum neutron exposure is independent of the functional form of the partial mixing. As long as the H/^{12}C profile decreases continuously from the H-rich envelope into the ^{12}C-rich intershell the neutron exposure is only dependent on the intershell ^{12}C abundance. For a larger ^{12}C abundance more ^{13}C is produced before it can effectively compete with ^{12}C for protons to make ^{14}N.

All this makes it necessary to treat the thermodynamic conditions in the star not as a static background, but instead to include the feedback of mixing processes, which are required for the s-process, back into the thermodynamic conditions. Lugaro et al. (2003b) made an important step into this direction and compared the effect of stellar evolution code input on the s-process predictions, in particular isotopic ratios, including $^{96}Zr/^{94}Zr$. One of the stellar evolution models includes mixing at the bottom of the PDCZ and predicts higher temperatures for the ^{22}Ne source (Section 3.2). The particular 3 $M_\odot$ model in conjunction with the nuclear reaction rates used in that paper lead to the conclusion that the mixing at the bottom of the PDCZ was too strong, because the predicted $^{96}Zr/^{94}Zr$ was higher than measured in the majority of grains. Clearly, the approach of Lugaro et al. (2003b) should be extended to a larger parameter space.

In the case of the $^{96}Zr/^{94}Zr$ ratio one is currently limited by the nuclear physics uncertainty. However, as better data will become available in the future, in particular on neutron capture rates of radioactive nuclei, the s-process will develop into a tool to probe physical processes in the stellar interior that affect the temperature and mixing properties.

The Zr example described here is only one of many branchings that can be used, all probing the stellar interior in a slightly different way. In some cases one is in fact not dependent on the experimentally difficult measurement of n–cross sections of radioactive species, like in the case of ^{128}I. Reifarth et al. (2004) examined the

branching between β^- and electron capture, which determines the ^{128}Xe/^{130}Xe ratio in SiC grains and in the solar system (where a small fraction of ^{128}Xe can be attributable to the p process). Neutron densities in AGB stars do not get high enough anywhere to activate the ^{128}I(n, γ) reaction. The half-life of ^{128}I is 25 min and dominated (95%) by the β^- decay. The electron capture is strongly temperature dependent in the temperature range covered by the PDCZ. At the bottom of the PDCZ where neutrons are released ^{128}I is produced but the electron capture rate at this location is too small to produce a ^{128}Xe/^{130}Xe ratio as low as measured in the SiC grains. Only at the lower temperatures in the top part of the PDCZ, where no neutrons are released, is the electron capture rate high enough to bypass ^{128}Xe. It is therefore required that ^{128}I produced at the bottom of the PDCZ is mixed to the cooler top on a timescale of the order of the decay time of ^{128}I. The convective turn-over timescale of the PDCZ is about 15 min according to the MLT.

In the model of Reifarth et al. (2004) a realistic convective mixing timescale in the PDCZ from stellar evolution calculations is used to model the transport of species between the hot bottom and the relatively cooler top of the PDCZ. With this approach they broadly confirm the convective mixing velocities.

It may be that the *s* process as a diagnostic tool is an astrophysical application, where the latest nuclear physics experimental reaction rate measurements will matter most. This application will also benefit from new analysis techniques that allow the measurement of isotopic ratios of many elements in the same grain, which could help breaking the degeneracy between mass and mixing effects.

4. OTHER CONSTRAINTS ON AGB EVOLUTION

As discussed in the previous section the physics of mixing in AGB stars is not well understood. In particular the connected roles of convection, overshooting, and rotation, and magnetic fields has not yet been studied sufficiently or at all for AGB stars. Theories for mixing owing to these processes that are applicable in 1D evolution calculations are usually derived in a local approximation. Examples are the MLT (Böhm-Vitense 1958) for convection, the work of Endal & Sofia (1976) for instabilities induced by rotation, or magnetic fields (Spruit 2002; MacDonald & Mullan 2004). The local theories of the effects of rotation and magnetic fields have not yet been fully evaluated in the context of AGB stars. However, such studies are important to identify the relative importance of the various effects in different regimes. The fundamental physical processes that cause mixing are either nonlocal or nonspherically symmetric or both.

4.1. Multidimensional Simulations

Multidimensional, multiphysics models address this problem. Most of the work in this regard focuses on compressible convection of stellar atmospheres and envelopes. Porter & Woodward (2000) simulated in 3D convective envelopes of giants covering more than four pressure-scale heights. Their simulations had

density contrasts around 11 and, accordingly, Mach numbers up to 0.8 were observed. Apart from the full treatment of hydrodynamics, the physics input was strongly simplified compared to modern 1D calculations. For example, they adopted an ideal gas equation of state and a constant thermal conduction to mimic the effect of radiation in the diffusion limit. Such simplifications are necessary to make explicit compressible convection simulations for near-sonic flows feasible. These large-scale simulations demonstrated the general applicability of the MLT to describe the averaged properties of convective heat transport inside the convection zone.

Other studies specifically focused on convective penetration and overshoot into the stable layers beyond the convective zone. Hulburt et al. (1994) studied the dependence of mixing into the stable region as a function of relative stability; they found both a penetration region, in which significant convective energy flux extends into the stable layers, and a subadiabatic overshooting layer, in which significant mixing can take place. Robinson et al. (2004) studied the upper convection-radiation transition layer for a solar and two sub-giant models and found that the overshooting distance increased from $0.5\,H_p$ for the solar model to $1.0\,H_p$ for the most evolved model. The overshooting flows carry little energy flux and do not change the subadiabaticity of the overshooting layer. Both of these findings were already noted by Freytag, Ludwig & Steffen (1996), who constructed 2D-radiation hydrodynamics simulations of shallow surface convection layers. They could analyse overshooting at the bottom and at the top of the convection zone as their sandwich-like setup included two stable layers enclosing the convectively unstable layer. Again, they find that average convective velocities decay smoothly and exponentially in the stable layers, thereby causing significant mixing outside the convectively unstable region. Similar results were found by Asida & Arnett (2000) when constructing 2D models of the oxygen-shell burning phase in massive stars. They too found exponentially decaying velocity fields in the stable layers, both above and below the shell. Convective oxygen-shell burning and convective helium-shell burning do have common properties. This study suggests convective shell burning will induce overshooting at the bottom and top (Section 3.2).

The multidimensional models cannot describe the entire star for any considerable length of evolution. It is well known that explicit compressible codes have to obey the Courant-Friedrich-Levy conditions that relate the time and spatial resolution via the sound speed. For the deep stellar interior, Mach numbers are usually small, and simulations in the anelastic approximation may be instructive (Kuhlen, Woosley & Glatzmaier 2003). Nevertheless, even such models would be currently restricted to parts of the star and time spans that may barely cover a local thermal relaxation timescale. Instead these multidimensional models can address individual aspects of certain physical processes. The information from these studies then has to be incorporated into recipies that can be included in 1D stellar evolution codes in order to predict actual observables. Herwig et al. (1997) have done this by implementing an exponentially decaying diffusive overshooting applied to all convective boundaries and derived from the calculations of Freytag, Ludwig &

Steffen (1996). Young et al. (2003) derived a formula for extra mixing based on the internal gravity wave concept, but equally based on multidimensional simulations. In the future the iteration of ever-improving multidimensional models with observations and 1D stellar evolution modeling will be a major driver for progress in this area.

## 4.2. Progenitors and Progeny of AGB Stars

Even as multidimensional models become more complete and sophisticated, 1D stellar-evolution calculations will remain the most important tool to study the evolution of AGB stars. With this approach large grids of evolution sequences in the mass-metallicity plane can be computed. One can then compare the effect of a particular prescription of some physics processes to stars of both high and low mass. For example, Heger, Langer & Woosley (2000) calculated the evolution of rotating massive stars that end their lives as neutron stars. According to their calculations, the final neutron stars were spinning much faster than required by observations of young millisecond pulsars. One explanation is a missing mode of angular momentum transport in the models. Langer et al. (1999) presented the first models of rotating AGB stars and used the same prescription of rotation as Heger, Langer & Woosley (2000). They found a core rotation velocity of 28 km/s. This is much higher than the range of $0.1 < v/\mathrm{km\,s}^{-1} < 1$ according to asteroseismology of white dwarfs (Section 3.2), hinting again at a missing process of angular momentum transport. The similarity of these two results for the prescription of rotation in stellar evolution, one for massive stars and one for AGB stars, is reassuring and, at the same time, reaffirms for both cases that the physical prescription is still incomplete. On the basis of the work of Spruit (2002), Herwig (2004a) speculated that angular momentum transport by magnetic field coupling may be the correct answer to the inconsistencies found in AGB stars. Heger, Woosley & Spruit (2004) have in fact carried out evolution calculations for massive stars including the magnetic instabilities described by Spruit (2002). They found that magnetic fields can have the desired effect. In their models, the rotation rate of the final collapsing iron core is reduced by a factor of 30 to 50 compared to the case without magnetic fields, alleviating much of the discrepancy between predicted and observed spin rates of young millisecond pulsars.

Another advantage of 1D calculations as opposed to multidimensional models is to compute full time sequences from the pre–main sequence through all evolution phases up to the AGB and beyond into the post-AGB and finally the white dwarf evolution regime. A given implementation of a physical process can then be tested by considering the effect during subsequent evolution phases. The observationally well-studied abundance anomalies in globular cluster members are associated with extra mixing in RGB stars. Observations show that mixing of burning products from the H shell up into the convective envelope leads to carbon depletion and nitrogen enhancement on the surface of upper RGB stars. Denissenkov & VandenBerg (2003) investigate rotation-induced turbulent diffusion and find that generally rather more mixing is required than predicted by rotational instabilities

corresponding to observed rotation rates. This seems to be at odds with the finding that much less rotational mixing, and core rotation, is required to accommodate the *s* process in AGB stars and rotation rates of white dwarfs. Eventually, a satisfactory description of mixing in stars should account for observational properties of RGB stars, AGB stars, and white dwarfs.

Finally, consequences of mixing processes in the AGB stellar interior may become observable at a later time, leading to additional important constraints on the evolution of AGB stars. Here we refer to the large body of observations of H-free or very H-deficient central stars of planetary nebulae as well as very young white dwarfs (Koesterke 2001, Werner 2001, Hamann et al. 2003). In short, about 25% of all stars that leave the AGB to evolve into white dwarfs will, in one way or another, loose all their small remaining H-rich envelope mass of the order $10^{-4} M_\odot$ and expose the bare H-free cores (Iben 1984). The C-, O-, and He-rich nature of these objects is evident from their Wolf-Rayet or PG 1159 type line spectra (Figure 8). These low-mass cousins of the massive Wolf-Rayet stars display in a similar way the interior, nuclear-processed material that has been built up during the stars' previous evolution. The more evolved representatives of this branch of post-AGB evolution appear as PG 1159 stars, equally showing large amounts of He and C, and smaller but significantly enhanced oxygen abundance. Although the members of these two groups show some diversity, the general abundance pattern can be summarized as follows: In mass fractions, He $\sim$ C $\sim$ 0.4 and O = 0.08 . . . 0.15.

These two classes of H-deficient stars are important for AGB evolution as they provide a unique opportunity to study directly the nuclear processing shells in AGB stars. Early attempts to explain the evolutionary origin focused on the born-again evolution scenario (Iben et al. 1983, Iben & MacDonald 1995). The star evolves off the AGB, becomes a H-rich central star and, eventually, a very hot, young white dwarf. However, the He shell may still be capable of igniting a late
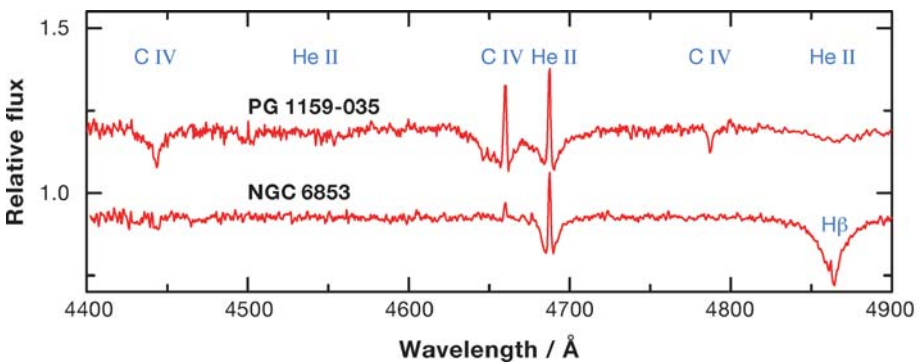
Figure 8 Spectra of H-deficent (*top*, *red star* in Figure 1) and H-normal (*bottom*, *green star* in Figure 1) hot central stars of planetary nebulae (courtesy Klaus Werner, University Tübingen, Germany).

He-shell flash. This event, estimated to occur in about one quarter of all central stars, will reverse the evolution back to the giant star configuration (Figure 1). In some cases the remaining H in the envelope is ingested into the He-shell convection zone (see HIF in Section 6.2). This case is the very-late pulse. As a result of H ingestion into the He convection and rapid burning, or by mixing from the emerging convective envelope (or because of both), the surface abundance of such born-again stars will be extremely H deficient or even H free (Blöcker 2001).

Stellar models of this evolutionary origin scenario connect the surface abundance of the Wolf-Rayet central stars and the PG 1159 stars with the intershell abundance of the progenitor AGB star. The intershell layer between the He and the H shell is well-mixed during each He-shell flash. This pulse-driven convection zone hosts important nucleosynthesis processes. It develops a unique abundance pattern, which is determined by repeated He burning on the ashes of H-shell burning that are periodically replenished by the complex sequence of mixing events in thermal-pulse AGB stars. The initial models of the H-deficient central stars by Iben and collaborators showed qualitatively that the born-again scenario could account for high He and C abundances, as these elements were abundant in the intershell of the AGB-progenitor model they used. However, they could not account for the high observed oxygen abundance. Herwig et al. (1997) were the first to propose that the solution could be nonstandard mixing during the AGB evolution. Models with overshooting at the bottom of the pulse-driven convection zone do not only feature higher temperatures at the bottom of the PDCZ (Section 3.2), but they also show higher C and, in particular, O abundances. Subsequently, Herwig (2000) explored in detail how the various abundances depend on the overshoot efficiency and other details. In essence, overshooting brings AGB intershell abundances of He, C, and O in very good quantitative agreement with the observed abundances of Wolf-Rayet–type central stars and PG 1159 stars, in the framework of the born-again evolution (Blöcker 2001, Herwig 2001b). More effort is needed to consolidate these constraints on the intershell abundance with the possibly tight upper limits on overshooting at the bottom of the PDCZ that the *s* process may provide (Section 3.2).

The connection of the surface abundances of the hot PG 1159 stars and the progenitor-AGB intershell abundance has been reinforced recently by several new observational findings. Miksa et al. (2002) found that FUSE spectra of two PG 1159 stars (K 1-16 and NGC 7094) showed Fe deficiencies of at least 1 dex compared to solar. If the PG 1159 stars show the progenitor-AGB intershell on their surface, then this Fe deficiency has a natural explanation. As discussed in Section 3, the intershell during the He-shell flashes (the PDCZ) is the site of the ^{22}Ne neutron source *s* process in AGB stars. Fe is the seed material for the *s* process, and the intershell has been exposed repeatedly to high neutron fluxes. Some Fe has been replenished via dredge-up processes (which are, for the case of Fe, rather a dredge-down). Models predict that Fe is depleted in the intershell by a factor of a few to 10, depending on the particular model. Further depletion of Fe may occur during the

actual formation of H deficiency when H is convectively ingested into the He shell. This can create additional ^{13}C as a source of neutrons leading to a last localized neutron irradiation during the very late thermal pulse. The result is a significantly reduced Fe abundance in H-deficient PG 1159 stars. In addition, stellar matter that has been subjected to significant neutron irradiation will show a depleted Fe/Ni ratio ($\sim 1 \dots 3$) corresponding to a local steady state that is determined by the (averaged) neutron cross section ratio of Fe and Ni and is much smaller than the solar ratio of $(Fe/Ni)_{\odot} = 20$.

This interpretation of the Fe deficiency finds support in the observed Fe/Ni ratio in Sakurai's object. This born-again star is the best-observed and most recent example of the very late thermal-pulse scenario and links this evolutionary scenario with the H-deficient PG 1159 and Wolf-Rayet–type central stars (Duerbeck et al. 2000, Herwig 2001a, Hajduk et al. 2005). Much of the observed abundance pattern of Sakurai's object as well as the rapid evolutionary timescale has been reproduced quantitatively with stellar models (Asplund et al. 1999, Herwig 2001a). Similar to the PG 1159 stars, Sakurai's object shows Fe depletion of about 1 dex compared to solar. The low ratio of $(Fe/Ni) = 3$, demonstrates that Sakurai's object shows surface material that has been directly irradiated with neutrons (Herwig, Lugaro & Werner 2002).

In addition to the Fe deficiency more new observations have recently strengthened the case that the observable surface layers of H-deficient PG 1159 stars are in fact nuclear-processed intershell material of the AGB progenitor. Werner et al. (2004) report a substantial overabundance of Ne on the basis of FUSE spectra of PG 1159 stars. These new observations confirmed previous results at shorter wavelength, which actually resulted in a quantitative neon abundance determination of 2% by mass (Werner & Rauch 1994). Evolution models of the intershell of low-mass AGB stars consistently predict a ^{22}Ne abundance of 2% by mass, which serves as an *s*-process neutron source. However, in low-mass AGB stars only a small fraction of the ^{22}Ne is burned. ^{22}Ne is the result of 2 α captures on ^{14}N that is repeatedly brought into the He shell by the interplay of dredge-up and the pulse-driven convection. In fact, ^{22}Ne in the intershell can accumulate to more than the combined CNO abundance of the initial composition as some of the ^{14}N that enters the He shell is made from ^{12}C dredged up during preceding thermal pulse cycles.

Another element that was recently observed in PG 1159 stars and found to confirm the notion that these stars display the intershell of the progenitor-AGB stars is fluorine. Werner, Rauch & Kruk (2005) observed highly ionized lines of F in the far-UV and determined abundances ranging from solar up to 250 times solar. This corresponds very well with the detailed analysis of fluorine nucleosynthesis in AGB stars by Lugaro et al. (2004). The F intershell abundances according to their models are large enough to cover even the largest F abundances observed in the extremely hot post-AGB stars. However, according to the nucleosynthesis and mixing analysis based on stellar-evolution models by Lugaro et al. (2004), the intershell abundance of F is diluted too much when dredged up into the envelope

of the AGB star in order to reproduce the observed relation between F and C/O in AGB stars (Jorissen, Smith & Lambert 1992) quantitatively. Lugaro et al. (2004) speculate that extra mixing as invoked in RGB-star models (see above) may also be operating in AGB stars. If that is correct, the missing fluorine is not made in the intershell of AGB stars but by partial H burning. The fluorine observations of PG 1159 stars lend support to that view. They confirm that the fluorine prediction for the AGB intershell are quantitatively correct and that, therefore, the quantitative discrepancy with AGB observations (the F-C/O relation) has to originate in missing additional processes.

5. THE FATE OF SUPER-AGB STARS: ONeMg WHITE DWARF OR NEUTRON STAR?

Super-AGB stars are massive enough to ignite C burning (García-Berro & Iben 1994). Therefore they do not evolve into CO white dwarfs[3] but rather form an ONeMg core. Super-AGB stars can end their lives either as massive ONeMg white dwarfs with masses in excess of $\sim 1 \, M_\odot$ or, alternatively, they may core collapse into neutron stars if they manage to grow their core mass beyond the Chandrasekhar mass (Ritossa, García-Berro & Iben 1999 and references therein). What fraction of super-AGB stars evolve into each of these channels and whether super-AGB stars can core collapse at all is still an open question. The mass range of super-AGB stars is defined by the formation of CO white dwarfs at the lower end of $\sim 8 \, M_\odot$ and by the disappearance of the second dredge-up at masses above $\sim 10 \, M_\odot$. Without second dredge-up that penetrates into the core below a mass coordinate of $1.37 \, M_\odot$, stars will not develop electron-degenerate cores and eventually end their lives as Fe-core-collapse supernova. Both upper and lower boundaries of this range are still uncertain and likely dependent on metallicity. They also depend on core overshooting, semiconvection, and other physics that affect the evolution of the H- and He-burning cores.

The core collapse that may end the lives of super-AGB stars is a possible site for the r-process in a neutrino-driven wind. The other two sites are the collapse of the Fe core of stars with initially $> 10 \, M_\odot$ and the accretion-induced collapse of a white dwarf in a binary with a low-mass companion. The proposal that there are, in fact, two distinct r-process sites is based on the analysis of r-process element-enriched stars, in particular at extremely low metallicity (Qian & Wasserburg 2003). In this picture one is responsible for the production of the heavy r-process nuclei with $A > 130$. Observations indicate that this r-process is not related to the production of the Fe-group elements or lighter elements from Na to Ti. This excludes the Fe core collapse as a source for this r-process as they have extensive shells containing these elements surrounding the Fe core. Fryer et al. (1999) analyzed the nucleosynthesis

---

[3]The well-known binary star Sirius B is a white dwarf of mass $M = 1.034 \pm 0.026 \, M_\odot$ (Holberg et al. 1998). Observations and stellar models agree that Sirius B has a C/O core and a massive AGB-star progenitor.

associated with the collapse of a white dwarf, and concluded that, because of the excess production of Sr, Y, and Zr, these events have to be rare. Although these calculations were done with the accretion-induced collapse in mind, they are also indicative of the collapse of a super-AGB star, should its core grow sufficiently during the shell-burning phase.

Whether or not super-AGB stars explode as core-collapse supernova depends on the interplay of mass loss and core growth. After the second dredge-up the super-AGB star has a core mass somewhat below the crititical core mass for core collapse (1.37 $M_\odot$). In order to explode, the core has to grow up to that critical core mass within the available time. The available time is given by the ratio of envelope mass and mass loss. If mass loss is large, the envelope will be lost before the core has grown enough and an ONeMg white dwarf will develop. If the mass loss is low, there is a chance to grow the core sufficiently to explode as a supernova. However, AGB evolution for such high core masses and maybe low or extremely low metallicity have some features that may complicate the situation. Modern full stellar-evolution models including a detailed network and updated input physics are not yet available for these stars. But we can express some expectations by analogy to the most massive AGB stars with CO cores that have been studied in detail. Recent models show that massive AGB stars have very efficient third dredge-up as well as hot-bottom burning (Karakas, Lattanzio & Pols 2002; Herwig 2004c). From these models it is also known that hot-bottom burning is more efficient at larger core masses. Very efficient hot-bottom burning can reduce the rate of core-growth. Hot-bottom efficiency depends on the physics of convection, which is uncertain in this regard (Section 2.5). Other peculiarities regarding the dredge-up in massive and very low-metallicity stars are addressed in Section 6. Finally, the massive, extremely low-metallicity AGB models predict significant primary production of Mg (Herwig 2004c), which may be a further constraint on the ability to generate the heavy r-process in this scenario without any of the lighter elements.

These are some of the open issues of super-AGB evolution models. Massive white dwarfs ($M > 1 M_\odot$) are observed (Należyty & Madej 2004). These could be the white dwarf endpoint of super-AGB evolution. White dwarf mergers would also result in such very massive white dwarfs. Strictly from the AGB evolution point-of-view, it appears possible that most super-AGB stars end their lives as ONeMg white dwarfs. It is interesting that this notion is consistent with the conclusion by Fryer et al. (1999) that the collapse of ONeMg white dwarfs is probably a rather rare event.

6. AGB EVOLUTION AT EXTREMELY LOW METALLICITY

In particular the increasing number of extremely low-metallicity stars (Beers & Christlieb 2005) has spurred interest in the evolution of AGB stars with extremely low or even zero metallicity.

6.1. Zero Metallicity

Several studies have addressed the evolution of intermediate mass stars at zero metallicity in recent years. However, the initial-mass function of Pop III stars may exclusively be populated at high or very-high masses (for a discussion see for example Chieffi et al. 2001), and $Z = 0$ AGB stars may not have really existed. Nevertheless, some aspects of $Z = 0$ stellar-evolution models (Chieffi et al. 2001; Siess, Livio & Lattanzio 2002) apply to ultra-metal-poor stars as well. These studies demonstrate that though the initial thermal pulses may show peculiar convective mixing events at the core–envelope boundary after the actual He-shell flash, eventually these stars enter a phase of rather normal thermal-pulse AGB evolution.

Many of the peculiarities of $Z = 0$ stellar evolution are due to the absence of CNO catalytic material for the H burning via the CNO cycle. During H-core burning, nuclear energy must be produced via the pp-chain, at least initially. This requires a higher temperature than H burning via the CNO cycle. With time the triple-α process can produce a small amount of C. A C mass fraction of 10^{-10} is sufficient to switch H-core burning to CNO cycling, and the $Z = 0$ stars will end H-core burning in this way. Then, during He-core burning some C is in fact produced even outside the convective core, and a tail of carbon reaches from the convective core out toward the H shell.

After the end of He-core burning, and depending on the initial mass, this C and some N is mixed into the envelope. According to Chieffi et al. (2001), this second dredge-up ($Z = 0$ as well as massive, extremely metal-poor–AGB stars do not have a first dredge-up) raises the C abundance in the envelope above 10^{-7} $M_\odot$ for $M_{ini} > 6$ $M_\odot$. For such a C abundance, the H-shell is fully supported by CNO cycling. As a result the thermal-pulse–AGB evolution is like that of the extremely metal-poor cases, featuring the well-known thermal-pulse cycle including the pulse-driven convection zone (PDCZ), dredge-up, and hot-bottom burning.

The initially less-massive cases than 6 $M_\odot$ do not dredge up enough C material to immediately follow a rather normal thermal-pulse–AGB evolution. Instead, both Chieffi et al. (2001) and Siess, Livio & Lattanzio (2002) report that, following a couple of weak prepulses, a H-shell convection zone forms immediately after the He-shell flash. This H convection zone is bounded at the bottom by the opacity discontinuity associated with the core-envelope interface. This convective boundary is highly unstable, and even small amounts of mixing will drive flash-like burning and deep mixing as protons enter a ^{12}C-rich zone. The details of the evolution of the H-shell convection zone is not important as this one-time event leads to deep dredge-up and enrichment of the envelope with an amount sufficient to support regular CNO cycle burning in the H shell thereafter. Accordingly, these lower-mass cases will evolve like extremely metal-poor stars too, and the $Z = 0$ models discussed here can be used as proxies for what is in reality born as ultra-metal-poor stars.

It is likely that the rotationally induced mixing processes in low- and intermediate-mass stars described for metallicity $Z = 10^{-5}$ by Meynet & Maeder (2002)

also apply to evolution models at lower metallicity and even $Z = 0$. In these models, ^{12}C and ^{16}O is mixed out of the He-burning core and up to the location of the H shell. There most of it is burned into ^{14}N and later picked up by the second dredge-up. The primary ^{14}N with an envelope-mass fraction of 10^{-4} should result in a normal thermal-pulse evolution without any peculiar H convection zone.

After some evolution on the thermal-pulse AGB the only difference between a real Pop III and an extremely metal-poor star would be the absence of Fe and other elements heavier than Al in the first one. Contrary to the initial intuition, this does not mean that a Pop III AGB star could not perform any s processes. Goriely & Siess (2001) tentatively applied the s-process postprocessing concept established for higher (solar-like) metallicities (Section 3.1) to $Z = 0$. They used the models of Siess et al. (2002) as stellar-evolution input and assumed that a ^{13}C pocket would form in the same way it is assumed to in solar-like metallicity models. Although this assumption is wrong (Herwig 2004b, Goriely & Siess 2004), the exercise is still instructive as it demonstrates that, if a sufficient neutron source is available, the s process can equally well be based on seed nuclei with lower mass number than Fe, for example C. One of the obvious signatures of an s process in a Pop III star would then be a strongly subsolar Fe/Ni ratio, approximately close to the steady-state value of ~ 3 that is given by the ratio of the neutron cross sections of Ni and Fe (the isotopic minimum for each element).

However, such a signature has not yet been observed. The most metal-poor star observed to date is HE 0107-5240 with [Fe/H]$= -5.3$ (Christlieb et al. 2004). This shows that low-mass stars can form at this ultra-low metallicity. AGB-evolution models for extremely and ultra-metal-poor stars should therefore be constructed for metallicities down to $Z = 10^{-7}$. HE 0107-5240 has an extreme nonsolar abundance pattern, characterized by large overabundances of C, N, O, and Na. All of these elements can be produced in large quantities in AGB stars of extremely low or even zero metallicity. The Fe/Ni ratio in HE 0107-5240 ([Ni/Fe]$= -0.2$), however, is almost twice the solar ratio, and a Pop III–AGB source of these heavy elements can clearly be excluded. Thus, though ultra-metal-poor–AGB stars have existed, there is no observational evidence for Pop III AGB stars.

6.2. The Hydrogen-Ingestion Flash

AGB models with $5\,M_\odot$ and $Z = 0$ by Herwig (2003a) showed the peculiar H-convective episode described above (Section 6.1) at the ninth thermal pulse, after 8 weak prepulses. However, in those models another well-known sequence of events is observed during the following thermal pulse. As the PDCZ grows, it eventually reaches out into the H-rich envelope. Protons are then mixed into the convectively unstable He-shell flash region, which is increasingly hot with depth. This leads to a hydrogen-ingestion flash (HIF), super-positioning the ongoing He-shell flash. A HIF was also found in the $2\,M_\odot$, $Z = 0$ model, but Herwig (2003a) did not find the HIF in models of $Z \geq 10^{-5}$.

The HIF in thermal-pulse AGB (TP-AGB) stars of extremely low or zero metallicity has been reported before by Fujimoto, Ikeda & Iben (2000). The higher temperature in the H shell of $Z = 0$ or very low-metallicity AGB stars leads to a smaller entropy barrier. In the initial mass range $1.0 \leq M/M_\odot \leq 3.0$ they find the HIF up to a metallicity of $Z \sim 10^{-4}$. For larger masses, represented by their $4\,M_\odot$ case, they do not find a HIF, nor is there a third dredge-up. In this latter regard, these results are in stark contrast to the results of Chieffi et al. (2001), Siess, Livio & Lattanzio (2002), and Herwig (2003a) for $Z = 0$, and Herwig (2004b) for AGB models at $Z = 10^{-4}$. Maybe Fujimoto, Ikeda & Iben (2000) had not followed the evolution for the $Z = 0$ sequence over enough pulses. This would explain the discrepancy in dredge-up predictions of massive AGB stars at $Z = 0$ as all three other studies found a number of about 8 weak prepulses without dredge-up preceding the stronger following pulses. However, at $Z = 10^{-4}$ Herwig (2004b) reports efficient dredge-up starting at the second dredge-up, differing from the models by Fujimoto, Ikeda & Iben (2000).

This discussion shows that there is currently some confusion about whether or not the HIF occurs in real stars and under which conditions. The heterogeneity of modeling results in this regard is related to the fact that AGB stars are highly nonlinear systems. The occurrence of the HIF depends on many details of the models, including the physics of mixing, opacities, the numerical resolution, and nuclear reaction rates. Small changes in any of these ingredients, that may go unnoticed during a more robust stellar-evolution phase (like the main sequence), can be the deciding factor during the AGB phase whether a HIF occurs or not. Note that stars experiencing the rotationally induced mixing during the pre-AGB phase described in Section 6.1 (Meynet & Maeder 2002) would in no case evolve through a HIF event, because the envelope would be sufficiently enriched with CNO (in particular N) material that serves as a catalyst for H burning.

If the HIF occurs in extremely metal-poor or zero-metallicity stars, it should reveal itself through distinct observational signatures. Iwamoto et al. (2004) explore possible implications of a HIF in terms of nucleosynthesis. Signatures may, for example, be related to the s process. Hydrogen ingested into the PDCZ may lead to ^{13}C production, which could release neutrons. Suda et al. (2004) propose that the abundance pattern of the currently most metal-poor star—HE 0107-5420—is in part due to the nucleosynthesis in thermal-pulse AGB stars with HIF. The details of the nucleosynthesis in a HIF depend sensitively on the physics of simultaneous rapid nuclear burning and convective mixing. The HIF can also be a source of lithium, distinctly different from conditions during hot-bottom burning (Herwig & Langer 2001a).

In Section 4.2 the evolution of born-again stars, like Sakura's object, has been described, because these objects provide valuable additional constraints for the evolution of AGB stars. The very late thermal pulse, which is triggering the born-again evolution, is in fact associated with a HIF. Models of Herwig et al. (1999) were, however, not able to reproduce the very short evolutionary timescale of the return of Sakurai's object. Herwig (2001a) showed that models in which the

convective H ingestion occurs with lower velocities than predicted by MLT feature a faster born-again evolution than MLT models, quantitatively in agreement with observations. The physical interpretation is that rapid nuclear burning on the convective timescale releases energy and adds buoyancy to down-flowing convective bubbles, leading to additional breaking of the plumes. The temperature and timescales for nucleosynthesis during the HIF would be significantly different. This has not yet been applied to HIF models at $Z = 0$ or extremely low metallicity.

6.3. AGB Nucleosynthesis at Extremely Low Metallicity

AGB stars are capable of producing a surprising number of species in a primary mode, meaning only from the initial H and He. However, at moderate metal deficiency or solar metallicity, the corresponding overabundance factors are often small. This is, for example, the case for oxygen, as discussed in Section 2.4, and overabundances for such species are not observed in stars of solar-like metallicity. However, this is different at extremely low metallicity. The initial envelope mass fraction of oxygen for models with $Z = 10^{-4}$ is $<5 \cdot 10^{-5}$. But the PDCZ abundance of ^{16}O is primary and, even at this low metallicity, of the order 1% by mass, even if no overshooting is assumed. Dredge-up of such material enhances the envelope abundance significantly.

A set of low- and intermediate-mass AGB stellar-evolution models with $Z = 10^{-4}$ ([Fe/H] $= -2.3$) with detailed structure, nucleosynthesis, and yield predictions has been presented by Herwig (2004c). The oxygen overabundance in these models is $\log(X/X_\odot) = 0.5 \cdots 1.5$, depending on mass. Other elements with sometimes significant primary production include C, N, Ne, Na, Mg, and to a lesser extent Al. With respect to C and N, it is important to point out that in standard AGB evolution either one of those is produced, depending on mass, i.e. on the occurence of hot-bottom burning. The abundance pattern of many C-rich and s-process-enriched extremely metal-poor (EMP; C-EMPs) stars with simultaneous large overabundances of C and N, like CS 29497-030 with [C/Fe] $= 2.4$ and [N/Fe] $= 1.9$ (Sivarani et al. 2004) is not predicted for a single AGB mass. The onset of efficient hot-bottom burning that turns almost all dredged-up C and O into N with mass is abrupt, somewhere around 3.5 $M_\odot$ for $Z = 10^{-4}$. More massive AGB stars have large N overabundance and relatively smaller C overabundance in their ejecta, and vice versa for low-mass AGB stars.

The elemental primary production of Ne and Mg of extremely metal-poor AGB stars is almost exclusively in the neutron-heavy isotopes. As described above, ^{22}Ne in AGB stars is primary. The low-mass stars do not burn this isotope much and have a ^{22}Ne overabundance of >2.5 in their cumulative ejecta.

For the primary production of the heavy Mg isotopes another effect specific to AGB stars at extremely low metallicity becomes important. With a primary neutron source (independent of inital metallicity) and a relatively smaller abundance of species, both light and heavy, that can capture neutrons, the s process leads to some

important nuclear production of light neutron-heavy species. ^{25}Mg is produced via the ^{22}Ne(α, n) reaction. The neutron captures on ^{22}Ne and ^{25}Mg lead to significant production of ^{23}Na and ^{26}Mg and determine their overproduction.

In the previous section it was argued that, owing to the large primary production of CNO and many other species, the $Z = 0$ model predictions would also apply approximately to stars with ultra-low metallicity. The neutron capture rates play such an important role that they have to be accounted for, together with a neutron-sink approximation for species not explicitly included in the network. This has been done in a qualitatively similar way by both Herwig (2004c) for the $Z = 10^{-4}$ models and Siess, Livio & Lattanzio (2002) for their $Z = 0$ models. It is then reassuring that the results are similar. For example, comparing the abundance evolution along the 2 $M_\odot$, $Z = 0$ and the 3 $M_\odot$, $Z = 10^{-4}$ cases, one cannot find qualitative differences. Both models predict large primary production of C and O. The $Z = 0$ model reaches a ^{14}N mass fraction of about 10^{-5} made in the early H convection zone (Section 6.1), whereas the $Z = 10^{-4}$ model has about the same ^{14}N abundance initially. In both cases this ^{14}N abundance does not change. ^{22}Ne is produced in both cases in the He-shell flashes, and in both cases the final ^{22}Ne exceeds that of ^{14}N. The evolution of ^{23}Na, ^{25}Mg, and ^{26}Mg is qualitatively the same too. In particular, the ratio of these three isotopes is quantitatively the same in the last computed model of the $Z = 0$ sequence and the final AGB model at $Z = 10^{-4}$. This is especially interesting as these low-mass AGB models predict that ^{26}Mg:^{25}Mg > 1, contrary to the signature of hot-bottom burning.

The agreement of the two different calculations indicates that some of the peculiarities of extremely metal-poor AGB evolution are treated correctly. However, there remain many open questions at this point. For example, Herwig (2004b) has shown that convection-induced extra mixing, like exponential overshoot that is used to generate a ^{13}C pocket for the *s*-process in higher metallicity models, may lead to vigorous H burning during the third dredge-up. Depending on the efficiency of such mixing, the third dredge-up may turn into a flame-like burning front, leading to very deep core penetration. The formation and effectiveness of a ^{13}C pocket may be significantly impacted (Goriely & Siess 2004).

7. CONCLUSIONS

A consistent theme throughout this review has been that the problems in understanding the physics of mixing is the main obstacle to substantial quantitative improvement of AGB evolution models and the associated nuclear yields. Several options have been discussed that may help to improve the situation. An improvement is badly needed, otherwise we may not be able to take full advantage of the swelling stream of high-quality and -quantity spectroscopic data, in particular from the regime of extreme metal deficiency as well as from extra-galactic stellar populations. It is suggested that the new era of spectroscopic surveys and multiobject fiber-optics spectrographs is complemented with a corresponding quantitative

effort in stellar evolution and nucleosynthesis. Particular effort is required in pursuing the implementation and adaption of nonstandard mixing processes induced by the combined action of convection, rotation, and magnetic fields. In addition, the direct multidimensional simulation of processes that occur in stars can support these efforts. The greatest immediate challenge is to help unravel the secrets that the most metal-poor stars still keep, in particular, those that appear to show signatures of pollution by AGB stars.

ACKNOWLEDGMENTS

The *Annual Review of Astronomy and Astrophysics* is online at
http://astro.annualreviews.org

LITERATURE CITED

Alexander D, Ferguson J. 1994. *Astrophys. J.* 437:879

Allende Prieto C, Lambert DL, Asplund M. 2002. *Astrophys. J. Lett.* 573:L137

Anders E, Grevesse N. 1989. *Geochim. Cosmochim. Acta* 53:197

Angulo C, Arnould M, Rayet M, Descouvemont P, Baye D, et al. NACRE Collab. 1999. *Nucl. Phys. A* 656:3

Arlandini C, Käppeler F, Wisshak K, Gallino R, Lugaro M, et al. 1999. *Astrophys. J.* 525:886

Asida SM, Arnett D. 2000. *Astrophys. J.* 545:435

Asplund M, Lambert DL, Kipper T, Pollacco D, Shetrone MD. 1999. *Astron. Astrophys.* 343:507

Bahcall JN, Pinsonneault MH. 2004. *Phys. Rev. Lett.* 92:121301

Battinelli P, Demers S. 2004. *Astron. Astrophys.* 418:33

Beer H, Voss F, Winters RR. 1992. *Astrophys. J. Suppl.* 80:403

Blöcker T. 1999. In *IAU Symp. 191: Asymptotic Giant Branch Stars*, p. 21

Blöcker T. 1995. *Astron. Astrophys.* 297:727

Blöcker T. 2001. *Astrophys. Space Sci.* 275:1

Blöcker T, Schönberner D. 1991. *Astron. Astrophys.* 244:L43

Böhm-Vitense E. 1958. *Z. Astrophys.* 46:108

Boothroyd AI, Sackmann I-J. 1988. *Astrophys. J.* 328:671

Boothroyd AI, Sackmann I-J, Ahern SC. 1993. *Astrophys. J.* 416:762

Boothroyd AI, Sackmann I-J, Wasserburg GJ. 1994. *Astrophys. J.* 430:77

Bowen GH. 1988. *Astrophys. J.* 329:299

Busso M, Gallino R, Lambert DL, Travaglio C, Smith VV. 2001. *Astrophys. J.* 557:802

Busso M, Gallino R, Wasserburg GJ. 1999. *Annu. Rev. Astron. Astrophys.* 37:239

Canuto VM, Mazzitelli I. 1991. *Astrophys. J.* 370:295

Chieffi A, Dominguez I, Limongi M, Straniero O. 2001. *Astrophys. J.* 554:1159

Christlieb N, Gustafsson B, Korn AJ, Barklem PS, Beers TC, et al. 2004. *Astrophys. J.* 603:708

Cox JP, Giuli RT. 1968. *Principles of Stellar Structure*. New York: Gordan & Breach

Denissenkov PA, Herwig F. 2003. *Astrophys. J. Lett.* 590:L99

Denissenkov PA, Tout CA. 2002. *MNRAS* 340:722

Denissenkov PA, VandenBerg DA. 2003. *Astrophys. J.* 593:509

Duerbeck HW, Liller W, Sterken C, Benetti S, van Genderen AM, et al. 2000. *Astrophys. J.* 119:2360

Eggleton PP. 1972. *MNRAS* 156:361

Endal AS, Sofia S. 1976. *Astrophys. J.* 210: 184

Forestini M, Arnould M, Lumer E. 1991. *Astron. Astrophys.* 252:127

Forestini M, Arnould M, Paulus G. 1991. *Astron. Astrophys.* 252:597

Forestini M, Charbonnel C. 1997. *Astron. Astrophys. Suppl.* 123:241

Forestini M, Goriely S, Jorissen A, Arnould M. 1992. *Astron. Astrophys.* 261:157

Freytag B, Ludwig H-G, Steffen M. 1996. *Astron. Astrophys.* 313:497

Frost CA, Cannon RC, Lattanzio JC, Wood PR, Forestini M. 1998. *Astron. Astrophys.* 332: L17

Frost CA, Lattanzio JC. 1996. *Astrophys. J.* 473: 383

Fryer C, Benz W, Herant M, Colgate SA. 1999. *Astrophys. J.* 516:892

Fujimoto MY, Ikeda Y, Iben I Jr. 2000. *Astrophys. J. Lett.* 529:L25

Gallino R, Arlandini C, Busso M, Lugaro M, Travaglio C, et al. 1998. *Astrophys. J.* 497: 388

García-Berro E, Iben I Jr. 1994. *Astrophys. J.* 434:306

Goriely S, Mowlavi N. 2000. *Astron. Astrophys.* 362:599

Goriely S, Siess L. 2001. *Astron. Astrophys.* 378:L25

Goriely S, Siess L. 2004. *Astron. Astrophys.* 421:L25

Habing HJ, Olofsson H, eds. 2004. *Asymptotic Giant Branch Stars*. Springer: Astron. Astrophys. Libr.

Hajduk M, Zijlstra AA, Herwig F, van Hoof PAM, Kerber F, et al. 2005. *Science* 308: 231

Hamann W-R, Gräfener G, Koesterke L. 2003. See Herwig et al. 2002, p. 203

Heber U, Napiwotzki R, Reid IN. 1997. *Astron. Astrophys.* 323:819

Heger A, Langer N, Woosley SE. 2000. *Astrophys. J.* 528:368

Heger A, Woosley SE, Spruit HC. 2004. ArXiv Astrophysics e-prints

Herwig F. 2000. *Astron. Astrophys.* 360:952

Herwig F. 2001a. *Astrophys. J. Lett.* 554:L71

Herwig F. 2001b. *Astrophys. Space Sci.* 275:15

Herwig F. 2003a. In *CNO in the Universe, ASP Conf. Ser.* astro-ph/0212366

Herwig F. 2003b. See Herwig et al. 2002, p. 61

Herwig F. 2004a. In *ASP Conf. Ser. 313: Asymmetrical Planetary Nebulae III: Winds, Structure and the Thunderbird*, p. 387

Herwig F. 2004b. *Astrophys. J.* 605:425

Herwig F. 2004c. *Astrophys. J. Suppl.* 155:651

Herwig F, Austin SM. 2004. *Astrophys. J. Lett.* 613:L73

Herwig F, Blöcker T, Langer N, Driebe T. 1999. *Astron. Astrophys.* 349:L5

Herwig F, Blöcker T, Schönberner D, El Eid MF. 1997. *Astron. Astrophys.* 324:L81

Herwig F, Langer N. 2001a. *Nucl. Phys. A* 688:221. astro-ph/0010120

Herwig F, Langer N. 2001b. In *Salting the Early Soup: Trace Nuclei from Stars to the Solar System*, ed. M Busso, R Gallino, p. 277. Mem. Soc. Astron. Ital. astro-ph/0007390

Herwig F, Langer N, Lugaro M. 2003. *Astrophys. J.* 593:1056

Herwig F, Lugaro M, Werner K. 2002. In *Planetary Nebulae. Their Evolution and Role in the Universe*, ed. M Dopita, S Kwok, R Sutherland, IAU Symp. 209. astro-ph/0202143

Holberg JB, Barstow MA, Bruhweiler FC, Cruise AM, Penny AJ. 1998. *Astrophys. J.* 497:935

Holweger H. 2001. *Solar and Galactic Composition*, ed. RF Wimmer-Schweingruber, AIP Conf. Proc. 598:23

Hurlburt NE, Toomre J, Massaguer JM, Zahn J-P. 1994. *Astrophys. J.* 421:245

Iben I Jr. 1984. *Astrophys. J.* 277:333

Iben I Jr, Kaler JB, Truran JW, Renzini A. 1983. *Astrophys. J.* 264:605

Iben I Jr, MacDonald J. 1995. In *White Dwarfs*, ed. D Koester, K Werner, LNP No. 443, p. 48. Heidelberg: Springer-Verlag

Iben I Jr, Renzini A. 1983. *Annu. Rev. Astron. Astrophys.* 21:271

Iglesias CA, Rogers FJ. 1996. *Astrophys. J.* 464:943

Itoh N, Hayashi H, Nishikawa A, Kohyama Y. 1996. *Astrophys. J. Suppl.* 102:411

Iwamoto N, Kajino T, Mathews GJ, Fujimoto MY, Aoki W. 2004. *Astrophys. J.* 602:378

Izzard RG, Tout CA, Karakas AI, Pols OR. 2004. *MNRAS* 350:407

Jorissen A, Smith VV, Lambert DL. 1992. *Astron. Astrophys.* 261:164

Karakas AI, Lattanzio JC. 2003. *PASA* 20:279

Karakas AI, Lattanzio JC, Pols OR. 2002. *PASA* 19:515

Kawaler SD. 2003. In *Stellar Rotation*, ed. A Maeder, P Eenens, IAU Symp. 215. astro-ph/0301539

Kingsburgh RL, Barlow MJ. 1994. *MNRAS* 271:257

Kippenhahn R, Weigert A. 1990. *Stellar Structure and Evolution*. Berlin: Springer-Verlag

Koester D, Dreizler S, Weidemann V, Allard NF. 1998. *Astron. Astrophys.* 338:612

Koesterke L. 2001. *Astrophys. Space Sci.* 275:41

Kuhlen M, Woosley WE, Glatzmaier GA. 2003. In *Astron. Soc. Pac. Conf. Ser.* 293:147

Lambert DL, Gustafsson B, Eriksson K, Hinkle KH. 1986. *Astrophys. J. Suppl.* 62:373

Langer N, Heger A, Wellstein S, Herwig F. 1999. *Astron. Astrophys.* 346:L37

Lattanzio JC. 1989. *Astrophys. J.* 344:L25

Lattanzio JC, Boothroyd AI. 1997. In *Astrophysical Implications of the Laboratory Study of Presolar Materials*, ed. T Bernatowitz, E Zinner, AIP Conf. Ser. 85

Ludwig H, Freytag B, Steffen M. 1999. *Astron. Astrophys.* 346:111

Lugaro M, Davis AM, Gallino R, Pellin MJ, Straniero O, Käppeler F. 2003a. *Astrophys. J.* 593:486–508

Lugaro M, Herwig F, Lattanzio JC, Gallino R, Straniero O. 2003b. *Astrophys. J.* 586:1305

Lugaro M, Ugalde C, Karakas AI, Görres J, Wiescher M, et al. 2004. *Astrophys. J.* 615:934

MacDonald J, Mullan DJ. 2004. *MNRAS* 348:702

Marigo P. 1998. *Astron. Astrophys.* 340:463

Marigo P. 2001. *Astron. Astrophys.* 370:194

Marigo P. 2002. *Astron. Astrophys.* 387:507

Marigo P, Bressan A, Chiosi C. 1996. *Astron. Astrophys.* 313:545

Marigo P, Bressan A, Chiosi C. 1998. *Astron. Astrophys.* 331:564

Marigo P, Girardi L, Bressan A. 1999. *Astron. Astrophys.* 344:123

Mazzitelli I, D'Antona F, Ventura P. 1999. *Astron. Astrophys.* 348:846

Meyer BS. 1994. *Annu. Rev. Astron. Astrophys.* 32:153

Meynet G, Maeder A. 2002. *Astron. Astrophys.* 390:561

Miksa S, Deetjen JL, Dreizler S, Kruk JW, Rauch T, Werner K. 2002. *Astron. Astrophys.* 389:953

Mouhcine M, Lançon A. 2002. *Astron. Astrophys.* 393:149

Mowlavi N. 1999. *Astron. Astrophys.* 344:617

Mowlavi N, Jorissen A, Arnould M. 1996. *Astron. Astrophys.* 311:803

Mowlavi N, Meynet G. 2000. *Astron. Astrophys.* 361:959

Należyty M, Madej J. 2004. *Astron. Astrophys.* 420:507

Nicolussi GK, Pellin MJ, Lewis RS, Davis AM, Clayton RN, Amari S. 1998. *Phys. Rev. Lett.* 81:3583

Paczyński B. 1977. *Astrophys. J.* 214:812

Pols OR, Tout CA. 2001. *Mem. Soc. Astron. Ital.* 72:299

Porter DH, Woodward PR. 2000. *Astrophys. J. Suppl.* 127:159

Qian Y-Z, Wasserburg GJ. 2003. *Astrophys. J.* 588:1099

Reifarth R, Käppeler F, Voss F, Wisshak K, Gallino R, et al. 2004. *Astrophys. J.* 614:363

Renda A, Fenner Y, Gibson BK, Karakas AI, Lattanzio JC, et al. 2004. *MNRAS* 354:575

Ritossa C, García-Berro E, Iben I Jr. 1999. *Astrophys. J.* 515:381

Robinson FJ, Demarque P, Li LH, Sofia S, Kim Y-C, et al. 2004. *MNRAS* 347:1208

Sackmann I-J, Boothroyd AI. 1992. *Astrophys. J.* 392:L71

Schönberner D. 1979. *Astron. Astrophys.* 79:108

Siess L, Goriely S, Langer N. 2004. *Astron. Astrophys.* 415:1089

Siess L, Livio M, Lattanzio J. 2002. *Astrophys. J.* 570:329

Sivarani T, Bonifacio P, Molaro P, Cayrel R, Spite M, et al. 2004. *Astron. Astrophys.* 413:1073

Smith VV, Lambert DL. 1990. *Astrophys. J. Suppl.* 72:387

Spruit HC. 2002. *Astron. Astrophys.* 381:923

Stancliffe RJ, Izzard RG, Tout CA. 2004. *MNRAS* 356:4

Stancliffe RJ, Tout CA, Pols OR. 2004b. *MNRAS* 352:984

Stolzmann W, Bloecker T. 2000. *Astron. Astrophys.* 361:1152

Straniero O, Chieffi A, Limongi M, Busso M, Gallino R, Arlandini C. 1997. *Astrophys. J.* 478:332

Suda T, Aikawa M, Machida MN, Fujimoto MY, Iben I Jr. 2004. *Astrophys. J.* 611:476

Travaglio C, Gallino R, Arnone E, Cowan J, Jordan F, Sneden C. 2004. *Astrophys. J.* 601:864

Travaglio C, Randich S, Galli D, Lattanzio J, Elliott LM, et al. 2001. *Astrophys. J.* 559:909

van Eck S, Goriely S, Jorissen A, Plez B. 2003. *Astron. Astrophys.* 404:291–99

van Winckel H. 2003. *Annu. Rev. Astron. Astrophys.* 41:391

van Winckel H, Reyniers M. 2000. *Astron. Astrophys.* 354:135

Vassiliadis E, Wood P. 1993. *Astrophys. J.* 413:641

Ventura P, D'Antona F. 2005. *Astron. Astrophys.* 431:279

Ventura P, D'Antona F, Mazzitelli I. 2002. *Astron. Astrophys.* 393:215

Ventura P, Zeppieri A, Mazzitelli I, D'Antona F. 1998. *Astron. Astrophys.* 334:953

Wachter A, Schröder K-P, Winters JM, Arndt TU, Sedlmayr E. 2002. *Astron. Astrophys.* 384:452

Wagenhuber J, Groenewegen MAT. 1998. *Astron. Astrophys.* 340:183

Werner K. 2001. *Astrophys. Space Sci.* 275:27

Werner K, Rauch T. 1994. *Astron. Astrophys.* 284:L5

Werner K, Rauch T, Kruk JW. 2005. *Astron. Astrophys.* 427:685

Werner K, Rauch T, Reiff E, Kruk JW, Napiwotzki R. 2004. *Astron. Astrophys.* 427:685

Willson LA. 2000. *Annu. Rev. Astron. Astrophys.* 38:573

Woosley SE, Heger A, Cumming A, Hoffman RD, Pruet J, et al. 2004. *Astrophys. J. Suppl.* 151:75

Woosley SE, Heger A, Weaver TA. 2002. *Rev. Mod. Phys.* 74:1015

Yoon S-C, Langer N, van der Sluys M. 2004. *Astron. Astrophys.* 425:207

Young PA, Knierman KA, Rigby JR, Arnett D. 2003. *Astrophys. J.* 595:1114

Zinner E. 1998. *Annu. Rev. Earth Planet. Sci.* 26:147

Contents

ERRATA
    An online log of corrections to *Annual Review of Astronomy and Astrophysics*
    chapters may be found at http://astro.annualreviews.org/errata.shtml